Progress in Particle and Nuclear Physics 67 (2012) 705–734

Contents lists available at SciVerse ScienceDirect

Progress in Particle and Nuclear Physics

journal homepage: www.elsevier.com/locate/ppnp

Review

The large hadron collider

O. Brüning *, H. Burkhardt, S. Myers

CERN, Geneva, Switzerland

ARTICLE INFO

Keywords:
Collider
Storage ring
Luminosity

ABSTRACT

The Large Hadron Collider (LHC) is the world's largest and most energetic particle collider. It took many years to plan and build this large complex machine which promises exciting, new physics results for many years to come. We describe and review the machine design and parameters, with emphasis on subjects like luminosity and beam conditions which are relevant for the large community of physicists involved in the experiments at the LHC. First collisions in the LHC were achieved at the end of 2009 and followed by a period of a rapid performance increase. We discuss what has been learned so far and what can be expected for the future.

Contents

1. Introduction 706
2. Basic design considerations 706
   2.1. Project goals 706
   2.2. Magnet design aspects 709
   2.3. Beam parameters for the nominal LHC 709
3. Injection 711
4. Machine protection 712
   4.1. Quench protection 713
   4.2. Beam loss protection 713
5. Interaction regions 714
   5.1. Colliding beams 716
6. Experience from commissioning and early operation 716
   6.1. Commissioning 716
   6.2. Early operation 719
   6.3. Progress in 2010 719
   6.4. Operational performance in 2010 722
   6.5. Proton operation in 2011 723
   6.6. Plans for the end of 2011 and 2012 725
7. Upgrade considerations 725
   7.1. Upgrade motivation and planned stages 725
   7.2. The HL-LHC upgrade goals 726
   7.3. Summary of the HL-LHC performance reach 732
   7.4. Summary 732
   Acknowledgments 733
   References 733

* Corresponding author.
E-mail address: oliver.Bruning@cern.ch (O. Brüning).

0146-6410/$ – see front matter © 2012 Elsevier B.V. All rights reserved.
doi:10.1016/j.ppnp.2012.03.001

1. Introduction

The LHC is the world's largest and highest-energy particle accelerator. As illustrated in Fig. 1, it is installed in an underground tunnel of 27.6 km circumference on the Franco-Swiss border near Geneva, Switzerland. The tunnel was initially built for and previously used by the large e^+e^- collider LEP.

The LHC is built with two beam-pipes which cross at four interaction regions, see Fig. 2 [1]. This allows particles of the same charge – proton–proton or heavy ions – to be accelerated and collided.

The most important design parameters for an accelerator for particle physics are the maximum energy and luminosity that can be reached. High energy is required to allow the production of new, heavy particles, like the yet undiscovered Higgs particle predicted by the Standard Model of particle physics. High rate of event production is about equally important, to allow for a high flux of particles resulting in a sufficiently high number of collisions.

The collision rate $\dot{n}$ for a process of cross section σ is the product of the luminosity L and the cross section

$$\dot{n} = L\,\sigma\,. \tag{1}$$

Cross sections are usually given in units of barn (symbol b), where $1\ \mathrm{b} = 10^{-24}\ \mathrm{cm}^2 = 10^{-28}\ \mathrm{m}^2$.

The luminosity of a collider is determined by the particle flux and geometry [2]. For head-on collisions as illustrated in Fig. 3, the luminosity is

$$L = \frac{N_1\,N_2\,n_b\,f_{\mathrm{rev}}}{A}, \tag{2}$$

where N_1, N_2 are the number of particles per bunch in beam 1 and 2, n_b is the number of bunches, f_{rev} the revolution frequency and A the effective beam overlap cross section at the interaction point. For beams with Gaussian shape of horizontal and vertical r.m.s. beams sizes σ_x, σ_y colliding head on, we have $A = 4\pi\ \sigma_x\sigma_y$.

The main path to very high luminosities in the LHC is to use many bunches, nearly 3000, and to reduce the transverse beam size at the Interaction Points (IPs) by manipulations of the magnetic focusing system at top energy, the so called squeezing of the beams before the beams are brought into collisions. The r.m.s. beam size at the position s in the machine is

$$\sigma(s) = \sqrt{\epsilon\,\beta(s)} \tag{3}$$

where ϵ is an average beam quantity called emittance, which represents the beam size in transverse phase space. For simplicity, we have assumed here, that the "dispersion" (change of optics with momentum) is small, which is generally the case in the interaction regions. See Eq. (6) for the more general expression with dispersion. Strong quadrupole magnets are used around the interaction regions to focus the beams. They allow to obtain small values of the β-function at the interaction point (called β^*) resulting in small beam-sizes and high luminosity.

Synchrotron radiation from protons at LHC energies becomes noticeable but is not a limitation.

The maximum beam energy in the LHC, or more precisely the beam momentum p is given by the maximum bending field strength B, according to $p = B\,\rho$, where the bending radius $\rho = 2804$ m is essentially given by the tunnel geometry. Numerically, $p\ [\mathrm{GeV/c}] = B\ [\mathrm{T}]\ \rho\ [\mathrm{m}]/3.336$.

The LHC is built with superconducting NbTi magnets. The cross section of the main dipole magnets is shown in Fig. 4. They are operated at superfluid Helium temperature of 1.9 K, and allow fields up to $B = 8.33$ T and $p = 7$ TeV/c.

The main LHC parameters are listed in Table 1 and compared to its predecessor LEP [3] in its final running phase and the Tevatron [4]. The design LHC parameters for the magnetic field and beam intensity are particularly ambitious. The aim is to get the maximum energy and luminosity reachable with current technology.

2. Basic design considerations

2.1. Project goals

The idea of a proton–proton collider within the LEP tunnel was already considered at the very beginning of the LEP project. Discussions of the Large Hadron Collider (LHC) started as early as 1983 [5], long before the first electron–positron collisions took place in LEP in 1989. The LHC design parameters evolved significantly over the following 10 years in a continuous comparison and competition with the SSC project in the United States [6] leading to a tenfold increase of the LHC performance from the first design projections [7] to the nominal LHC performance specification [1].

The key objective of the LHC is the exploration of the Standard Model in the TeV energy range, the search for the Higgs Boson and potential new physics signatures. The LHC can be considered as a discovery machine, which uses collisions of hadrons. Collider storage rings can in principle be designed for a variety of particle species. Leptons are truly pointlike elementary particles and lepton colliders allow for a well defined collision energy and are well suited for precision measurements (e.g. LEP), but more limited in luminosity and maximum beam energy at comparable size and cost.

The energy limitation of electron rings from synchrotron radiation could in principle be overcome by using (short lived) muons rather than electrons. Muon colliders are being studied [8], but are at present very far from a technical realization.

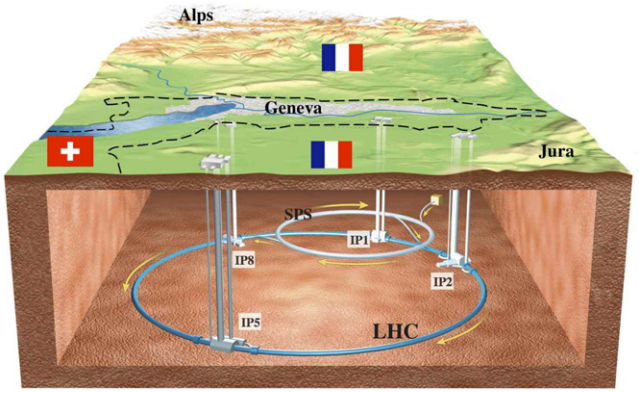

Fig. 1. Schematic diagram of the LHC collider with the SPS as injector and four interaction regions (IP).

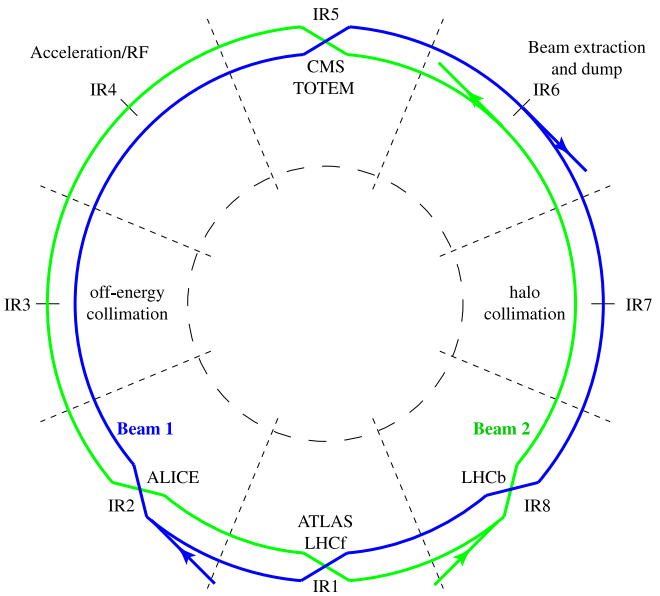

Fig. 2. Schematic layout of the LHC with its 8 arc sections, two-beam design and its four experimental insertions.

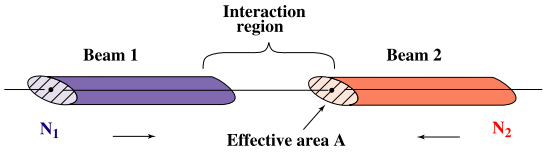

Fig. 3. Luminosity from particles flux and geometry.

Hadrons (e.g. protons and anti-protons) also allow for higher energies. However, they are not elementary particles but are rather composites of quarks and gluons. The collisions in a hadron collider are therefore collisions between quarks and gluons and the actual collision energy depends on the fraction of the total hadron energy that is carried by the colliding hadron constituents. Hadron colliders are the ideal instruments for the exploration of unknown territory as the collisions naturally cover a wide energy range. The relatively weak (as compared to lepton storage rings) synchrotron radiation in a circular hadron collider (the synchrotron radiation power is proportional to the cubic power of the relativistic gamma factor) provides another argument for using hadron rather then lepton beams in the LHC as this is compatible with the use of superconducting magnet technologies. A hadron collider offers the highest energy reach.

A circular collider project can follow two distinct design options: either the collider features collisions between particles and anti-particles with opposite charges, allowing an efficient accelerator design where both beams share the same vacuum chamber and magnetic elements (e.g. like LEP, the $Sp\bar{p}S$ [9] and the Tevatron collider) or the collider features separate

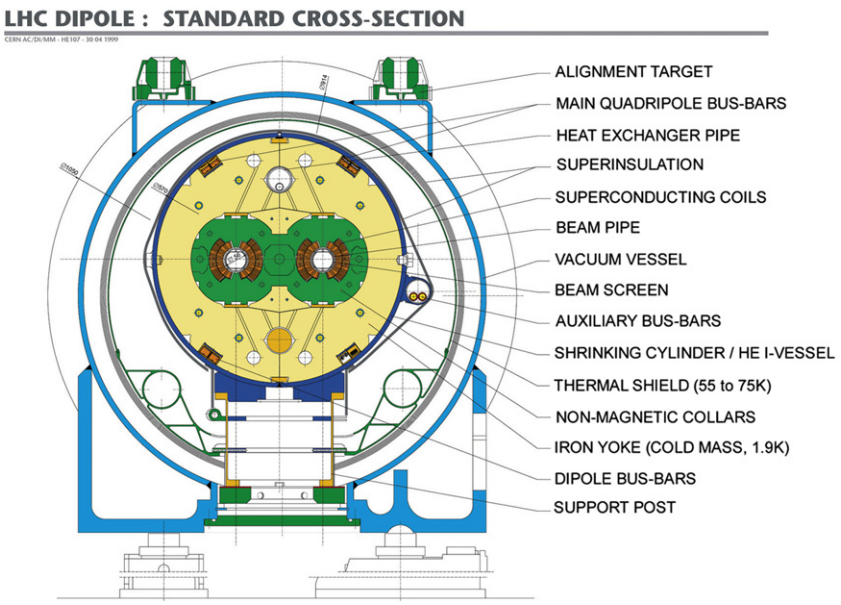

Fig. 4. Schematic cross-section of the LHC dipole magnet cryostat with its two separate vacuum chambers and magnet coils for the two counter-rotating beams and the common infrastructure for the powering and cooling of the magnet.

Table 1
Comparison of LHC and LEP2 design beam parameters.

	LHC	LEP2	Tevatron
Colliding beams of	p, p	e^+, e^-	$p, \bar{p}$
Momentum at collisions, TeV/c	7	0.1	0.98
Peak luminosity, $\mathrm{cm}^{-1}\ \mathrm{s}^{-2}$	10^{34} (design)	10^{32}	4.3×10^{32}
Dipole field at top energy, T	8.33	0.11	4.4
Number of bunches, each beam	2808	4	36
Total beam current/beam, A	0.58	0.003	0.08
Particles/bunch, 10^{11}	1.15	4.2	2.9, 0.8
Typical beam size in the ring, μm	200–300	1800/140 (H/V)	500
Beam size at IP, μm	16	200/3 (H/V)	24
Fraction of energy lost in synchr.rad. per turn	10^{-9}	3%	10^{-11}
Total power radiated in synchr.rad., MW	0.0078	18	10^{-6}
Total energy stored in each beam, MJ	362	0.03	0.9
Total energy stored in the magnet system, GJ	10	0.016	0.74

vacuum and magnet systems for the two counter-rotating beams (e.g. like the ISR [10], HERA [11] or RHIC [12] collider) allowing collisions between a wider range of particle species and larger number of bunches resulting in higher luminosity. Hadron colliders relying on particle and anti-particle collisions are intrinsically limited by the rate at which anti-particles can be generated. The high luminosity requirements (luminosities in excess of $L = 10^{33}\ \mathrm{cm}^{-2}\ \mathrm{s}^{-1}$) for the LHC excluded the use of anti-protons and therefore require a two ring design with separate magnet and vacuum systems for the two counter-rotating hadron beams. Designing the LHC with two separate magnet and vacuum systems for the two counter-rotating beams allows further the operation with more complex hadron species (e.g. ion beams). In order to minimize the infrastructure requirements, the LHC followed a novel 2-in-1 magnet design where the two apertures for the counter-rotating hadron beams feature separate magnet coils (and opposite field polarities) but share the same cryostat and powering infrastructure. Fig. 4 shows the schematic cross-section of the LHC dipole magnet cryostat with its two separate vacuum chambers and magnet coils for the two counter-rotating beams and the common infrastructure for the powering and cooling of the magnet.

The LHC has been designed with four experimental insertions: two insertions for high luminosity experiments (ATLAS [13] and CMS [14]) using proton–proton collisions ($L \geq 10^{34}\ \mathrm{cm}^{-2}\ \mathrm{s}^{-1}$), one B-meson experiment (LHCb [15]) requiring medium luminosities for proton–proton collisions ($L \propto 10^{32}\ \mathrm{cm}^{-2}\ \mathrm{s}^{-1}$) and one dedicated experiment for ion collisions (ALICE [16]) requiring low luminosities ($L \propto 10^{29}\ \mathrm{cm}^{-2}\ \mathrm{s}^{-1}$) for the operation with proton beams.

The use of protons implies that the collisions at the interaction points (IPs) occur actually between the constituents of the proton particles (Quarks and Gluons) which carry only a fraction of the total proton beam energy.

Aiming at TeV center of mass (CM) collision energies therefore requires proton beam energies well in excess of 1 TeV. The nominal LHC design aims at proton beam energies of 7 TeV.

2.2. Magnet design aspects

The LEP tunnel has a total circumference of 27.6 km, featuring ∼5 km of straight sections and space for dispersion suppression and 8 arc sections with a continuous curvature covering in total ∼22 km. However, a strong focusing synchrotron design cannot use all of the arc area for the installation of dipole magnets, since it requires dedicated quadrupole magnets for the stabilization of the particle trajectories and the transverse r.m.s. beam size in a synchrotron is directly related to the total transverse focusing strength. The distribution of the arc space between dipole and quadrupole magnets therefore implies a careful tradeoff between the achievable maximum dipole field and quadrupole gradients and the feasible maximum magnet aperture. For the LHC, this tradeoff led to the design of rather long dipole magnets (15 m), requiring a slightly curved magnet design with a 5 cm Sagitta (the long magnet design minimizes the number of required magnet-interconnection points) covering in total approximately 80% of the arc sections of the old LEP tunnel. Designing the LHC for a proton beam energy of 7 TeV with 80% of the LEP arc sections covered by dipole magnets implies a peak dipole field of 8.3 T which is at the limit of the existing NbTi superconducting magnet technology [17]. Fig. 5 shows the critical surface for superconducting cables made of NbTi [18]. The shaded surface indicates the 4.5 K operating point for NbTi superconducting material used in most other accelerator applications which is clearly incompatible with an operating magnet field of 8.3 T (no margin left for a significant current density J in the superconducting cables). The construction of superconducting magnets with a field strength in excess of 8 T and a non-vanishing current density in the cables (a realistic magnet design requires $J \sim 2\ \mathrm{kA/mm^2}$) therefore requires a magnet operation at temperatures close to 2 K. An operating temperature of 1.9 K has been chosen for the LHC where ^{4}He is superfluid and attains a large thermal conductivity. Both properties are key assets for an efficient cooling of the superconducting magnet coils.

2.3. Beam parameters for the nominal LHC

The instantaneous luminosity is given by

$$L = \frac{N_1 N_2 n_b f_{\mathrm{rev}}}{\pi \sqrt{(\sigma_{x,1}^2 + \sigma_{x,2}^2)}\sqrt{(\sigma_{y,1}^2 + \sigma_{y,2}^2)}} F H, \tag{4}$$

where f_{rev} is the revolution frequency, n_b the number of bunches colliding at the IP, $N_{1,2}$ are the number of particles and $\sigma_{x,1,2}$ and $\sigma_{y,1,2}$ the horizontal and vertical beam sizes of the colliding bunches. F is the geometric luminosity reduction factor due to collisions with a transverse offset or crossing angle at the IP and H is the reduction factor for the hour glass effect that becomes relevant when the bunch length is comparable or larger than the β-functions at the IP (the transverse β-function varies over the luminous region where the two beams interact with each other). Both factors can be combined to one luminosity reduction factor: $R = F H$.

The geometric reduction factor due to a crossing angle is given by:

$$F = 1 \Big/ \sqrt{1 + \left(\frac{\sigma_s}{\sigma_t}\frac{\phi}{2}\right)^2}, \tag{5}$$

where σ_s is the longitudinal bunch length, σ_t the transverse bunch size in the plane of the crossing angle and ϕ the total crossing angle.

In the following we assume that all bunches of both beams have equal intensities ($N_1 = N_2 = N_b$) and the same size at the IP. The transverse beam sizes at the IP are given by

$$\sigma_{x,y} = \sqrt{(\beta_{x,y}^* \epsilon_{x,y}) + D_{x,y}^2 \delta_p^2}, \tag{6}$$

where δ_p is the relative r.m.s. momentum spread ($\delta_p = \frac{\Delta p}{p_0}$) of the particles within a bunch, $\beta_{x,y}^*$ and $D_{x,y}$ are the horizontal and vertical β and dispersion functions at the IP and $\epsilon_{x,y}$ the horizontal and vertical emittances of the two beams. The beam emittance is a function of the beam energy and is often specified by the normalized beam emittance ϵ_n, which is entirely determined by the injector complex and the ability to preserve the beam emittance in the LHC over the full operation cycle:

$$\epsilon_n = \frac{\epsilon}{\beta\,\gamma}, \tag{7}$$

where γ is the Lorentz factor and $\beta = v/c$ ($\approx$1 at LHC energies) the velocity in units of the speed of light.

Assuming round beams at the IP and neglecting any spurious dispersion at the IP one can write the instantaneous luminosity in the LHC IPs as:

$$L = \frac{\gamma f_{\mathrm{rev}} n_b N_b^2}{4\pi\,\epsilon_n\,\beta^*} F. \tag{8}$$

Maximizing the instantaneous luminosity in the LHC therefore implies (in order of priority):

- Optimize the overlap of the two beams at the IP. For head-on collisions this implies simply a matching of the optics functions for the two beams and transverse steering of the beam orbits.

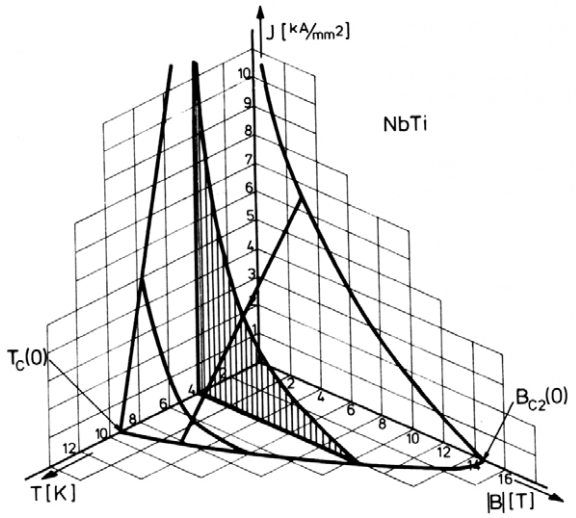

Fig. 5. The critical surface for NbTi superconducting cable within the 3 dimensional parameter space of Current density, peak magnetic field and temperature of the superconducting material.

- Minimize the beam size at the IPs (does not imply a "cost" in terms of total beam power but requires sufficient aperture and might imply special large aperture focusing quadrupole magnets near the experiments and tighter settings for the collimation system).
- Maximize the number of particles per bunch (increases linearly the total beam current and beam power but enters quadratically into the luminosity).
- Maximize the number of bunches in the collider (increases linearly the total stored beam power and the luminosity). For the LHC interaction region layout, the operation with more than 150 bunches requires the introduction of a crossing angle at the IP in order to avoid unwanted parasitic beam interactions left and right from the IP in the common vacuum beam pipe of the two beams.

The beam size at the IPs is limited by the smallest attainable beam emittance and the smallest attainable optical β-functions at the IPs. The beam emittance may be limited by the beam–beam interaction (beam brightness) and the performance of the injector complex of the LHC. The smallest attainable optical β-functions at the IPs are limited by the available aperture of the quadrupole magnets next to the IP and by chromatic aberrations in the LHC. The single bunch intensity is limited by collective effects [19] and by the strength of the non-linear beam–beam interaction that the particles experience when the bunches of both beams collide with each other at the IP [20,21]. The minimal bunch spacing and maximum number of bunches is constraint by multipactoring effects [22] like the electron-cloud effect [23] and the strength and number of acceptable parasitic long-range collisions in the common vacuum chamber of the two beams. The total beam current is eventually limited by hardware limitations and collective effects (e.g. multi-bunch instabilities). Another possible limitation of the instantaneous luminosity can be due to the existing hardware in the machine (e.g. the cooling capacity for the superconducting magnets of the triplet assembly) and by the detector performance (e.g. maximum permissible event pileup per bunch crossing). The optimization of the beam overlap for operation with crossing angles depends on the availability of novel accelerator technologies (e.g. Crab cavities and wires for the beam–beam compensation of long-range beam–beam effects). In any case, the potential performance gain via a compensation of the geometric reduction factor from the operation with crossing angles is only small for the nominal LHC parameters (ca. 10%) and becomes only interesting for operation with smaller β^* values (see Section 7.2).

Since the bunch intensities and beam sizes of a collider vary over time, the instantaneous luminosity is implicitly a function of time and the integrated luminosity, the measure for the total number of events generated in the collider over a period of time, is defined by

$$\hat{L}(t - t_0) = \int_{t_0}^{t} L(\tau) d\tau, \tag{9}$$

where t_0 is an arbitrary starting point, $L(\tau)$ the instantaneous luminosity at a given time and $t - t_0$ the time period of interest. In addition to the luminosity lifetime, the integrated luminosity depends strongly on the overall collider efficiency (ratio between the time spend in physics operation and the time required for preparing a new physics fill—also called "turnaround time") and the machine availability (depends on the number of scheduled operation days and days required for technical maintenance and the overall equipment fault rate).

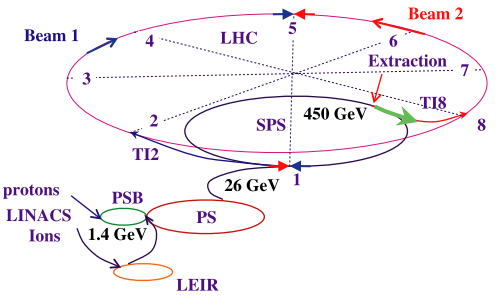

Fig. 6. Schematic view of the LHC with its injectors.

Table 2
Length (circumference), bending radius ρ and beam momentum at injection of the main accelerators in the LHC injection chain.

Machine	L (m)	Relative	ρ (m)	Beam momentum (GeV/c)	Bunches
LINAC	30		–	10^{-4}	4×2
PSB	157		8.3	0.05	4×2
PS	628.318	1	70.676	1.4	72
SPS	6911.56	$11 \times$ PS	741.257	26	4×72
LHC	26 658.883	$27/7 \times$ SPS	2803.98	450	2×2808

Table 3
Bunch intensity and normalized emittance at injection into the LHC.

	Design value	2011 operation
N particles/bunch	1.15×10^{11}	1.4×10^{11}
ϵ_n, μm	3.5	2

3. Injection

Filling the LHC with protons or ions requires a range of pre-accelerators. The first stage is a source and linear accelerator "LINAC", followed by the Booster (PSB), PS and SPS rings, see Fig. 6.

The size of these accelerators and their beam momentum at injection are listed in Table 2.

The radio frequency (RF) systems provide a longitudinal focusing which constraints the particle motion in the longitudinal phase space to a confined region called the RF bucket. The RF-frequency of the LHC is 400 MHz which corresponds to 75 cm wavelength or buckets of 2.5 ns length. The LHC circumference is 35 640 RF-wavelengths which would theoretically allow for the same number of buckets. Filling all buckets with particles would produce collisions spaced by only 37.5 cm.

A more realistic bunch spacing for the LHC is one per 10 RF-buckets or 25 ns. With a crossing angle of ∼0.3 μrad, this allows for $10\,\sigma$ beam separation for the parasitic beam encounters at multiples of 3.75 m from the interaction points (at the nominal β^*). A larger bunch spacing also reduces the unwanted multipactoring effects like the "electron cloud effect" mentioned earlier. Gaps of 225 ns corresponding to the injection kicker rise time are required between batches of bunches to fill the LHC. A single 3 μs gap is required to allow to cleanly dump the particles in the LHC. This limits the maximum number of bunches in the LHC per ring to 2808.

Table 2 also shows the maximum number of bunches for injection with 25 ns spacing in the LHC accelerator chain. Groups of bunches are called batches. The PS can inject batches of 72 bunches into the SPS. The SPS is filled with up to 4 PS batches.

The beam quality in the LHC is pre-determined by the injectors. The main figures of merit are the intensity, i.e. the number of protons or ions per bunch and the beam emittance ϵ_n. A small emittance corresponds to a high particle density and allows for high luminosity. Numerical values are given in Table 3. During acceleration, the transverse oscillation amplitudes decrease proportional to the square root of the momentum p ($\sigma \propto \sqrt{\epsilon}$, $\epsilon \propto \epsilon_n/\beta\gamma \propto \epsilon_n/p$, Eq. (7)).

The protons are injected through transfer lines TI 2, TI 8 into the LHC. Beam 1 is injected through TI 2 at point 2 of the LHC in clockwise direction. A schematic layout of this injection region is shown in Fig. 7. The focusing quadrupoles are labeled as Q. The incoming beam is directed by dipole magnets to the LHC. The MSI is a "septum magnet" in which the incoming beam is deflected by 12 mrad towards the circulating beam. The last active injection element is the pulsed kicker magnet MKI which deflects the incoming beam vertically by 0.85 mrad onto the orbit of the circulating LHC beam. In order to allow a proper injection setup with pilot bunches and to protect the LHC in case of malfunctioning of the injection kickers, an injection beam stopper, TDI, is placed 15 m upstream of the superconducting recombination dipole D1, supplemented by an additional shielding element, TCDD, 3 m upstream of D1.

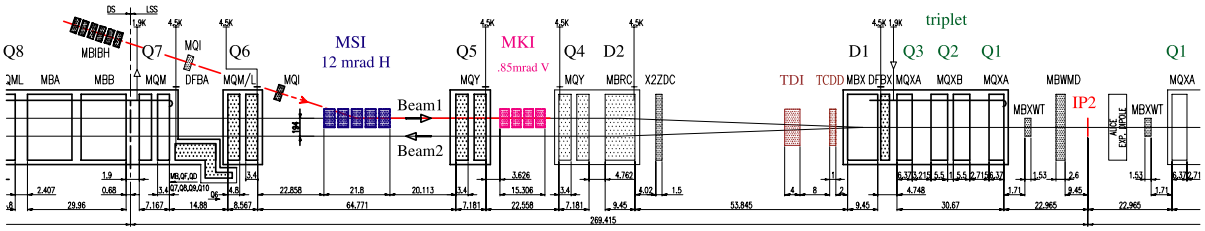

Fig. 7. Left side of IR2 with the injection region for LHC ring 1.

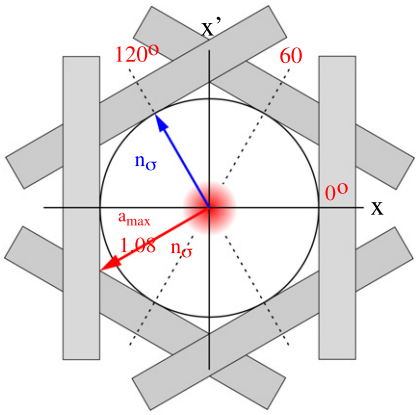

Fig. 8. Phase space coverage with 3-phase collimation at 0, 60, 120° in the transfer line.

Similarly, beam 2 is injected into the LHC through TI 8 at point 8 of the LHC in the opposite, counter-clockwise direction. The beams are kept separated by typically $\pm 6\,\sigma$ at the four IPs during all phases of preparation for colliding beams: injection, acceleration to the collision energy, and the reduction ("squeezing") of β^* to minimize the beam size to increase the luminosity for collisions.

Nominal LHC injection intensities require extraction of up to 4 batches with each 72 bunches or together 288 bunches of 1.15×10^{11} which makes a total of 3.3×10^{13} protons in 4/11 of an SPS turn or 7.86 μs. This intensity exceeds the damage level (about 2×10^{12}, see next section) by over one order of magnitude and the quench limit in the LHC (about 5×10^{9} protons) by nearly four orders of magnitude.

Several measures are taken to assure the clean and safe injection of high intensities into the LHC. High amplitude or "halo" particles are the first to get lost at aperture limitations and cause potential problems with losses, background and radiation. Halo particles contribute little to the luminosity and should be removed before they get into the superconducting LHC and further accelerated [24]. The efforts for clean injection start in the LHC injectors and in particular in the SPS, to assure that clean beams are extracted from the SPS and sent to the LHC [25,26].

The SPS is equipped with fast single sided, horizontal and vertical scrapers. They are moved close to the beams to remove halo particles above $\sim 3\sigma$. This is done at the end of the acceleration cycle to 450 GeV in the SPS, before the extraction of the protons into the transfer lines.

The next step is to assure the clean and safe transmission of these beams into the LHC. The TI 2 and TI 8 transfer lines between the SPS and LHC are each about 2.5 km long and comprise many normal conducting magnets running in pulsed mode. The transfer lines are equipped with a set of 3 vertical and horizontal collimators separated by 60° in betatron phase (see Fig. 8) to intercept halo particles at amplitudes above 4–5 σ at injection into the LHC and to minimize the risk of damage in the LHC by accidental beam loss or mis-steered beams at injection [27,28].

By design, the beams are injected in groups of 3 or 4 batches with up to 288 bunches in the LHC, allowing to fill 2808 bunches with 12 injection cycles per beam from the SPS. The particles are injected directly on the central design orbit in the LHC, longitudinally displaced to fill most of the LHC circumference. In practice, there is some ripple and unavoidable kicker jitter resulting in injection oscillations of $\sim 1.5\,\sigma$ [29]. The injection oscillations are damped using an active feedback system, to minimize the emittance increase at injection [30].

For injection and ramping up in energy, the LHC operates with optics which are optimized for maximum aperture with β values of ~10 m at the interaction points.

4. Machine protection

A major challenge in the LHC is the large amount of energy stored in the superconducting magnet system (10 GJ at the design energy) and in the circulating beams (362 MJ/beam, see Table 1) [1].

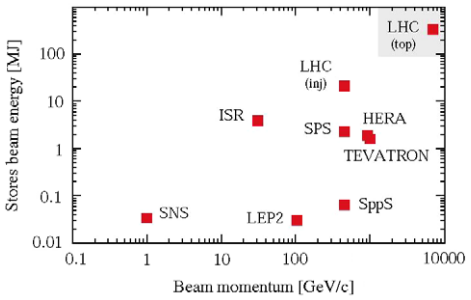

Fig. 9. Total stored beam energy versus beam momentum for various past and present high power accelerators.

The LHC is equipped with an active machine protection system designed to automatically turn off and safely extract the energy in the magnets and the beams in case of problems.

The LHC is also equipped with passive protection devices consisting of collimators and shielding blocks, designed to keep the more gradual unavoidable losses of protons during all operation phases away from the superconducting magnets.

4.1. Quench protection

A current of 12 kA is supplied to reach the design field of 8.33 T in the LHC dipoles. The inductance of a LHC dipole is typically $L = 100$ mH. The energy stored in a single dipole at full current is $I^2 L/2 = 7.2$ MJ which adds up to 1.1 GJ (Gigajoule) per sector or nearly 10 GJ for the LHC.

In case of a transition from super to normal conduction state – the quench – this energy has to be safely removed from the magnet system.

The first concern in quench protection is to avoid excessive energy deposition in the small zone, typically of the order of a few millimeters, where the transition to the normal state started. Quenches are detected as resistance increase causing a voltage rise over a magnet. For the LHC dipole circuits, a voltage rise by 100 mV over at least 10 ms represents a clear signal of a quench. Once a quench is detected, the first protection measure is to distribute the ohmic losses in the magnet over a larger area. This is done by triggering the discharge of a capacitor bank into resistors in the magnet, the "quench-heaters" which raise the temperature of the whole magnet coil by 10 K in 25 ms resulting in a global quench of the whole magnet.

The second measure is to safely discharge the quenched magnet and to provide a bypass for the current of the other magnets powered in series with the quenched magnet to avoid that these deposit their energy in the quenched magnet. For this purpose, all main superconducting magnets in the LHC are equipped with high-current bypass diodes. These diodes are connected in parallel to the magnet coil and operated at the same low temperature as the magnet coil. The turn-on voltage of the diodes increases at low temperature so that the current flows only through the superconducting coil. In the event of a quench, the temperature and resistance of the coil increases and the current flows through the diode.

4.2. Beam loss protection

The LHC has been designed for a beam intensity of 3.23×10^{14} protons at 7 TeV energy, which corresponds to a total energy of 362 MJ. This is much higher than in other machines, see Fig. 9. For comparison, the energy required to heat and melt 1 kg of copper is 0.7 MJ.

The total beam intensity is roughly 3 orders of magnitude above the damage level for direct beam impact. A beam intensity 100 times below the damage level is sufficient to quench the magnets, for localized losses in the superconducting sections of the accelerator.

The damage potential for direct beam impact was experimentally verified by fast extraction of the SPS proton beams at 450 GeV as used for LHC injection on to a stack of copper plates. The stack was exposed to four "shots" using different intensities and impact points. In Fig. 10 we can see, that an intensity of 8×10^{12} protons was sufficient to shoot a hole through the copper plate.

The LHC is equipped with a fast active beam loss and protection system. Beam losses are monitored by several thousand monitors all around the ring. The beam loss monitor thresholds are adjusted to trigger a beam abort, just below the beam loss level which would otherwise result in a beam loss induced quench of the magnets. At the injection energy of 450 GeV, the level for sudden beam losses which can lead to a quench is 5×10^9 protons and corresponds to the pilot beam bunch intensity used to establish circulating beams at injection. At top energy, a beam intensity two orders of magnitude smaller is sufficient to induce a beam induced quench.

The beams can be cleanly removed from the LHC by the beam dump system installed around LHC point 6. The beam dump system is equipped with fast (< 3 μs rise time) kicker magnets and allows to empty the LHC within a single turn. The particles leave the LHC through dedicated beam dump channels on either side of point 6. The beams are finally stopped

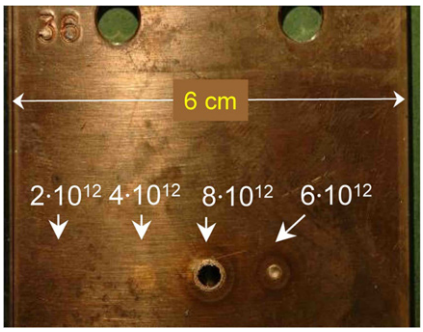

Fig. 10. Damage observed in controlled tests with perpendicular beam impact of 450 GeV protons from the SPS on copper.

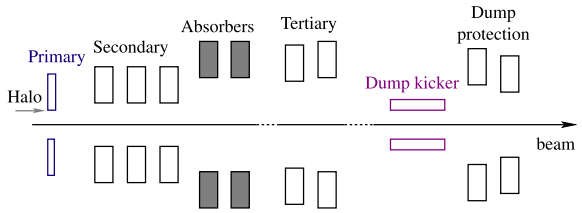

Fig. 11. Schematic view of the collimation hierarchy in the LHC.

in the ∼8 m long graphite core of the beam dump absorber which is surrounded by concrete and iron located at ∼700 m downstream from point 6.

The LHC is equipped with a three stage collimation system [31]. The collimation system is designed to remove halo particles in regular operation, to reduce the risk for damage and quenches of the superconducting equipment and to localize and minimize the impact of radiation and radioactive activation.

The main betatron or halo collimation system is installed at LHC point 7 (see Fig. 2) far from the experiments. The primary collimators are closest to the beam, typically at $\sim 6\sigma$ where σ is the nominal r.m.s beam size and cut the primary beam halo. These are two sided collimators with fiber-reinforced graphite (CFC) jaws and an active length of 60 cm, which was chosen as a compromise between robustness and cleaning efficiency. Secondary collimators intercept the secondary halo, i.e. the particles scattered by the primary collimators, and are typically placed 7–8 σ from the beam axis. The jaws are also made of CFC and have an active length of 1 m. The secondary collimators are followed by absorbers with copper jaws with a tungsten inlay, designed to catch the showers produced by these collimators at the end of each cleaning section.

Tertiary collimators are arranged around the experimental insertions, to catch remaining halo particles and to protect the triplets against mis-kicked beams.

A schematic view of the collimation hierarchy in the LHC is shown in Fig. 11.

An off-momentum cleaning section is installed around point 3 of the LHC (see Fig. 2). The primary collimator in IR3 is placed in a region with significant momentum dispersion to catch off-momentum particles which are then stopped by secondary collimators and absorbers.

Dump protection collimators are installed around point 6 of the LHC to protect against mis-kicked beams.

5. Interaction regions

The LHC layout has 8 arcs connected by 8 straight sections, approximately 528 m long. They are labeled as interaction regions IR 1 to IR 8 in the schematic Fig. 2. The beams cross in 4 of these, IR 1,2,5,8.

IR 1 and 5 are located on diametrically opposite sides of the LHC and house the high luminosity experiments ATLAS and CMS. On the LHC machine side, IR 1 and 5 are identical in terms of magnet layout and optics. An alternating crossing scheme is used to minimize the impact of the beam–beam effect. Beams cross in the vertical plane for IR 1 and in the horizontal plane for IR 5. The crossing angles are generated by dedicated dipole corrector magnets, which superimpose the crossing angle orbit excursion onto the central trajectories of beam 1 and 2.

The beams cross in the middle of the straight sections, except for IR8 where the crossing was shifted by 15 half RF-wavelength (11.25 m) to one side to provide sufficient space for the spectrometer magnet of the LHCb experiment.

The space ±23 m left and right of the interaction regions is reserved for the experiments.

Strong quadrupole magnets Q1–3 are installed symmetrically left and right of the experiments. The two LHC beams share the same beam pipe over the first ±60 m from the interaction point (IP) until they are horizontally separated by the separation dipole D1. A schematic view of the interaction region together with the first 171 m of the straight section on one side are shown in Fig. 12. From the recombination magnet D2 on, the two beams travel in parallel, separated horizontally by 194 mm.

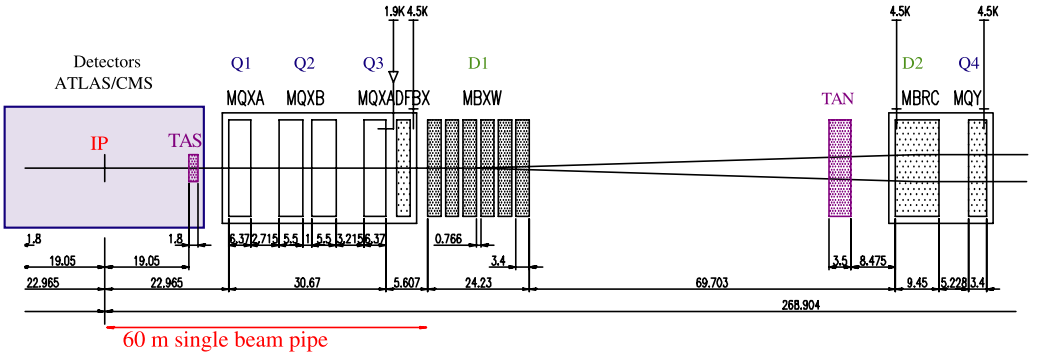

Fig. 12. Schematic layout of straight section on the right side of IR1 (and IR5)—up to Q4.

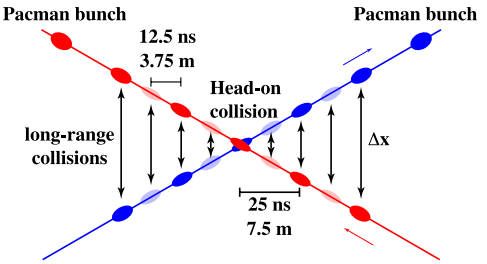

Fig. 13. Geometry with crossing angle. For 25 ns bunch spacing, long range encounters occur every 12.5 ns.

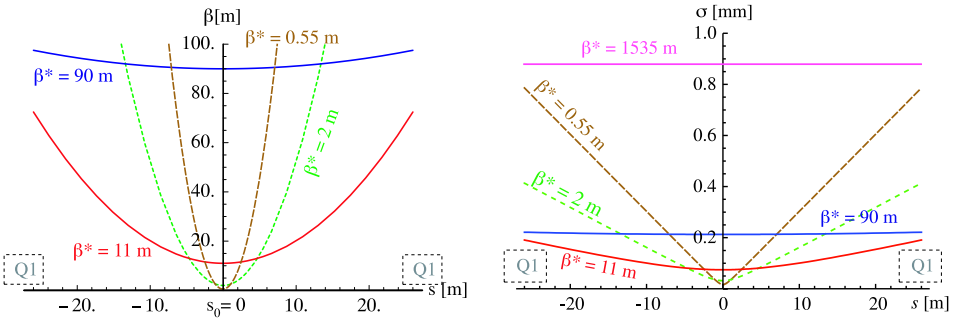

Fig. 14. Illustration of the β-functions (left), and beam sizes (right) around the IP at $s_0 = 0$ up to the center of the first quadrupoles Q1 at ± 26 m; for $\beta^* = 0.55$, 2, 11, 90 and 1535 m, for nominal beam parameters (at 7 TeV, $\epsilon_N = 3.75 \times 10^{-6}$ m, $\epsilon = 0.5$ nm).

By design, the LHC can be filled with bunches spaced by 25 ns or 7.5 m. The counter-rotating beams would cross at 3.75 m or 16 times left and right of the interaction region in the common region before the separation dipole D1. Using a set of dipole corrector magnets, the beams can be made to cross at an angle of ± 150 μrad to avoid the unwanted collisions in the common part of the beam pipe, see Fig. 13. The heading or trailing bunches of a batch which experience fewer long range encounters are also referred to as Pacman bunches. Fig. 12 also shows the position of two absorbers for the high rate of collision debris, the 1.8 m long copper absorber TAS at 19 m and the TAN at 143 m from the interaction point. The TAS (Target Absorber Secondaries) reduces the flux of secondary particles from the interaction point into Q1–Q3. The TAN (Target Absorber Neutrals) absorbs the flux of forward high energy neutral particles (neutrons, and photons) that are produced at the high luminosity interaction regions (∼200 W at design parameters).

The strong superconducting quadrupoles Q1–Q3 focus the beams transversely (in the horizontal or x direction, as well as in the vertical or y direction) to small beam sizes at the interaction points. The focusing properties of the magnetic lattice are described by β-functions. We recall, that beam sizes are related to β and emittance ϵ by $\sigma = \sqrt{\beta\epsilon}$, and that the emittance decreases with energy. In the LHC, we have on average $\beta_{x,y} \approx 100$ m in the arcs. The value of the β-function at the interactions point is called β^*. The low β triplet magnets Q1–3 have been designed to allow for a minimum of $\beta^*_{x,y} = 0.55$ m. Between the first focusing quadrupoles Q1 left and right of the interaction point, the horizontal and vertical β-functions are described by a parabola which has its minimum at the interaction point. The corresponding r.m.s beam sizes decrease linearly to the interaction points, see Fig. 14.

We can see that a smaller beam size at the interaction point ($\sigma \approx 17$ μm as required for high luminosity), results in a larger beam size in the triplet quadrupoles, of the order of $\sigma = 1$ mm. The increased beam sizes inside Q1–Q3, together

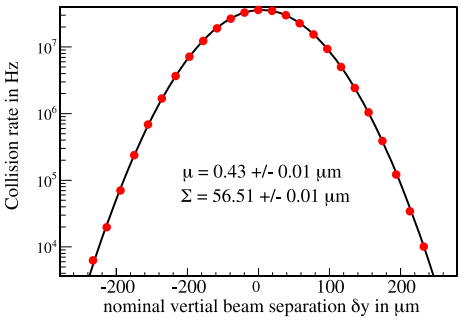

Fig. 15. Example of a vertical separation scan, performed on the 15 May 2011 in IP5. The dots represent the collision rate recorded on-line by the CMS experiment as a function of the nominal parallel vertical separation. The continuous line is the result of fitting a single Gauss curve to the data; μ and Σ are the fit values for the mean and width with their statistical uncertainty.

with the requirements for beam separation by $\sim 10\,\sigma$ and a minimum clearance of $\sim 10\,\sigma$ from the magnet aperture, limit the minimum attainable β^*.

The r.m.s angular beam divergence $\theta = \sqrt{\epsilon/\beta}$ increases when the beams are squeezed to small β^*, to 30 μm at the design parameters (7 TeV, 0.55 m). Special, high $\beta^* \sim 1500$ m optics have been developed to also allow for very low ∼0.5 μrad divergence beams as required for total cross sections measurements.

5.1. Colliding beams

The final step in the preparation for physics after injection, ramp and squeeze is to make the two beams colliding by turning off the parallel separation in the interaction regions.

The LHC is equipped with beam position monitors (BPM) and dipole steering magnets installed close to the quadrupoles around the ring. This allows to keep closed orbit deviations from alignment and magnet tolerances in the LHC below 0.5 mm. Pairs of correctors left and right the interaction regions at the Q4–Q6 quadrupoles are used to adjust the parallel horizontal and vertical separation at the interaction points. Collision rates from the experiments are sent to the LHC control room in frequent intervals (around once per second) and can be displayed as a function of the nominal transverse separation controlled by the steering magnets. Small scans in parallel separation using 3–5 points per plane over $\pm 0.5\,\sigma$ are routinely used to center the collisions for maximum luminosity. This is done initially when beam are brought into collisions and repeated after some hours to correct for small orbit drifts.

Fig. 15 shows an example of the luminosity recorded by an experiment (CMS) during a more extended scan in transverse beam separation.

For Gaussian distributions, the luminosity L as a function of the transverse separation is also Gaussian

$$L(\delta x, \delta y) = L(0,0)\ \exp\left[-\frac{\delta x^2}{2\,\Sigma_x^2} - \frac{\delta y^2}{2\,\Sigma_y^2}\right], \tag{10}$$

where

$$\Sigma_x = \sqrt{\sigma_{x,1}^2 + \sigma_{x,2}^2}, \qquad \Sigma_y = \sqrt{\sigma_{y,1}^2 + \sigma_{y,2}^2}$$

are the transverse widths of the overlap region of both beams at the interaction points. The extended scans provide a precise measurement of the beam overlap region and allow together with the beam intensities measured by beam current transformers for an absolute calibration of the luminosity provided by the LHC to a precision of ∼3.5% [32,33].

6. Experience from commissioning and early operation

6.1. Commissioning

The scheduled start-up with beam on September 10, 2008 was an overwhelming success. Both beams made a full machine turn within hours of the scheduled time, and one beam was captured by the RF system. Following this impressive beginning, a technical problem arose with an electrical transformer which necessitated stopping commissioning for a few days. During this stop it was decided to test the last octant (sector 34) up to 9.3 kA, the dipole current required for operation at 5 TeV per beam. At 8.7 kA a resistive zone developed in the dipole bus bar magnet interconnects. This led to thermal runaway in the interconnect, followed by the development of an electrical arc, initially across the interconnect, later puncturing the helium enclosure, and finally puncturing the beam pipes. The release of the helium caused a pressure wave over a region of more than 400 m resulting in damage to magnets, interconnects and pollution of the ultra-high vacuum system.

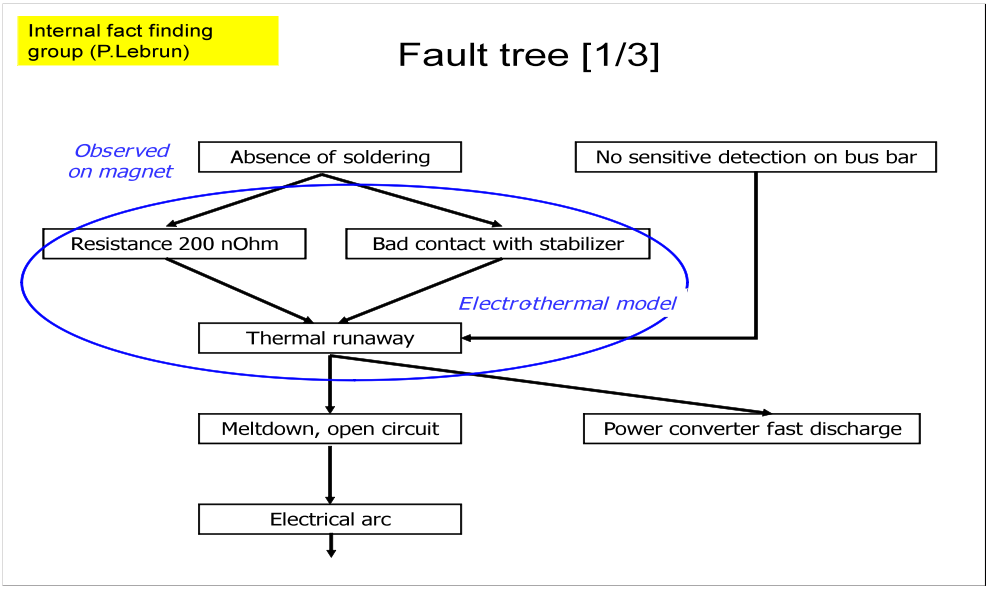

Fig. 16. Fault tree.

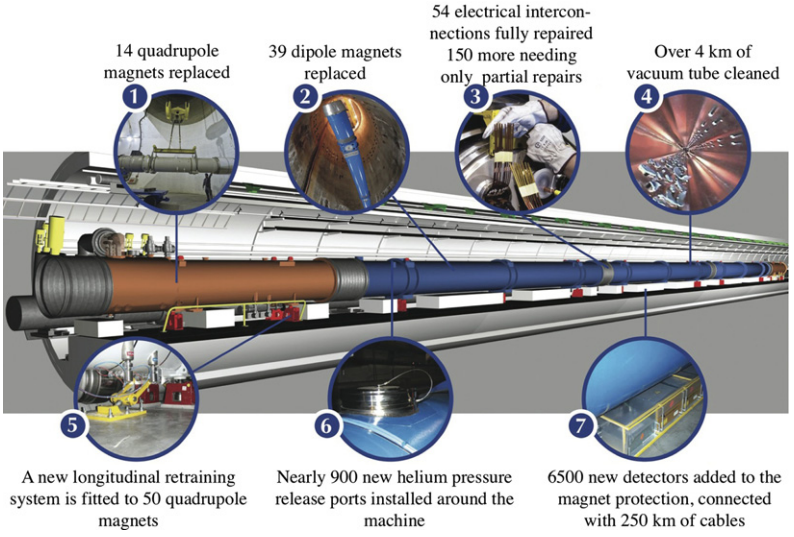

Fig. 17. Schematic of the main elements of the repair.

An inquiry by CERN specialists [34] indicated several causes of the substantial damage to the machine:

- there was an absence of solder on the offending magnet interconnect giving a contact resistance of 220 nΩ (design 1 nΩ);
- there was poor electrical contact between the superconducting (sc)cable and the copper stabilizing bus-bar;
- the fault detection of the interconnect was not sensitive enough;
- the pressure relief ports were under-dimensioned for an accident of this magnitude;
- the anchorage of the magnets to the tunnel floor was inadequate.

Fig. 16 shows the first page of a three page fault tree describing in detail the evolution of events immediately following the thermal runaway.

The repair

Following the initial investigation of the resulting damage, a crash program was set up to repair and consolidate the LHC. The teams included many CERN partners, collaborators, detector people as well as the accelerator sector. The task was enormous and required not only repair of the damaged components but equally importantly re-engineering many elements so that such an accident could never occur in the future.

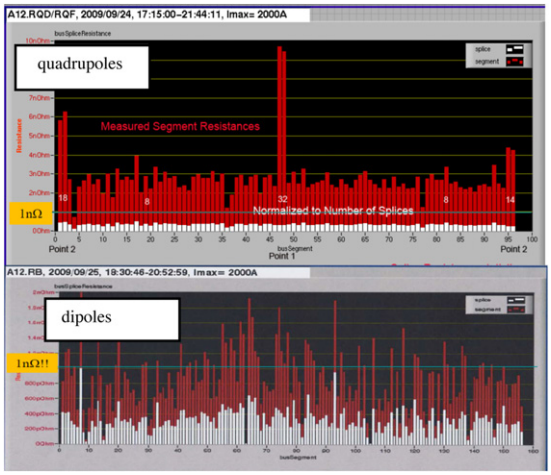

Fig. 18. Measurements of the resistance of the sc inter-magnet splice resistances (white lines are the calculated resistances of the splices).

Fig. 17 shows a schematic of the main elements of the repair in the damaged part of the tunnel. A total of 39 dipole magnets (marked 2 in diagram) were replaced. In addition, 14 quadrupole magnets were replaced (marked 1 in diagram) and a total of 54 damaged magnet interconnects needed full repair (marked 3) with around 150 extra (marked 3) needing partial repair. More than 4 km of ultra-high vacuum beam tube (marked 4) required the removal of small pieces of super-insulation and black soot followed by careful cleaning [35]. A new longitudinal restraining system (marked 5) was designed and installed on 50 quadrupole magnets. All existing flanges on the magnets were equipped with additional pressure relief ports (typically 10 cm diameter) and 20 cm flanges were cut on dipoles and equipped with double size pressure relief ports. In total 900 helium pressure relief ports were added (6).

A major task was the upgrade [36] of the magnet protection system which had been shown to be insensitive as a protection of the interconnect splices. The new design is 3000 times more sensitive (threshold reduced from 1 V to 0.3 mV) than the older system and involves 6500 new detectors marked (7)and the installation of more than 250 km of cable. A major added advantage of the new magnet protection system is that it gives the possibility of measuring [37], to sub-nΩ precision, the resistance of all inter-magnet splices in the machine (see Fig. 18 for results).

The copper stabilizer bus-bars

The completed inter-magnet bus-bar splice is designed for two separate functions. Firstly, at sc temperatures, to provide perfect electrical contact between the joined sc cable braids, and secondly, at non-sc temperatures (in the event of a quench for example) to ensure electrical continuity across the copper sheath. Hence in the event of a quench when the sc cable has a finite resistance, the copper sheath shunts the current away from the sc cable while the stored energy is being extracted from the magnet. In this way the sc cable is protected in case of a quench by the large cross-section of the copper stabilizer.

The procedure for producing an inter-magnet bus-bar is depicted in Fig. 19. The solder has two important functions, firstly to ensure good electrical contact between the two sc cable braids and secondly to ensure electrical continuity between the 2 copper profiles and the left and right copper sheaths (bus-bar). A little thought should indicate that if there is not electrical continuity across the copper stabilizer then the decaying current following a quench will flow through the sc cable (which is no longer superconducting) and possibly cause thermal runaway.

The quality of a splice is therefore determined by the resistance across the splice measured both at superconducting temperatures and at non-sc temperatures. Fig. 20 shows a photograph of a completed bus-bar as installed in the LHC.

The enhanced quality assurance introduced during the repair of sector 3–4 revealed new concerns about the copper bus bar in which the superconductor is embedded.

Tests demonstrated that the soldering process can cause discontinuities in the copper part of the bus-bars and produce voids which prevent contact between the superconducting cable and the copper stabilizer.

Consequently, in 2009, a campaign was started to measure the splice resistance [37] at room temperature. The "in-situ" measurement technique had a limited precision corresponding to about a factor of three higher than the resistance of a perfect splice. Consequently this technique could only be used to identify "outliers" which had a significantly increased resistance. On identification of outliers a much more precise measurement (which involved the overhead of opening the interconnect) could be performed. In this way all significant outliers were identified and repaired. However the limited precision of the "in-situ" measurement implied that some splices may have resistances significantly above the design value. Calculations, simulations and experimentation revealed that the maximum current that can flow in the interconnects without causing thermal runaway was less than the currents needed for maximum beam energy. Consequently it was decided to operate the LHC (for a limited period) at a safe energy compatible with the existing situation of the already installed splices.

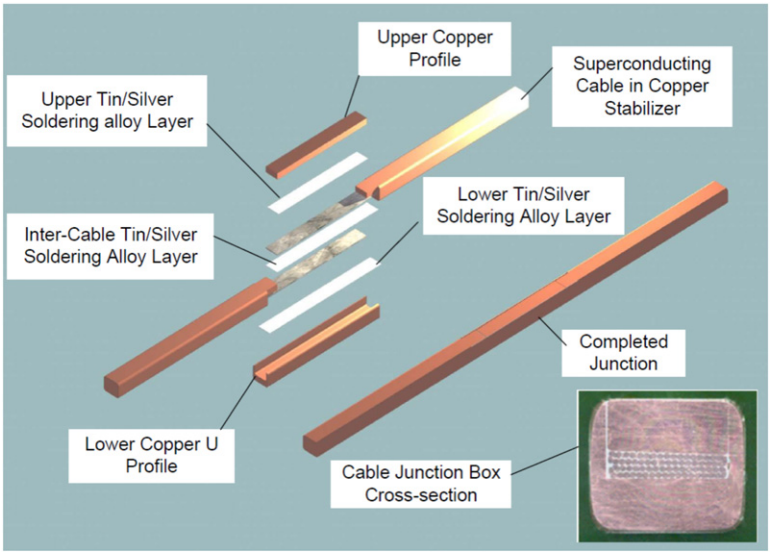

Fig. 19. Exploded diagram of an inter-magnet bus-bar.

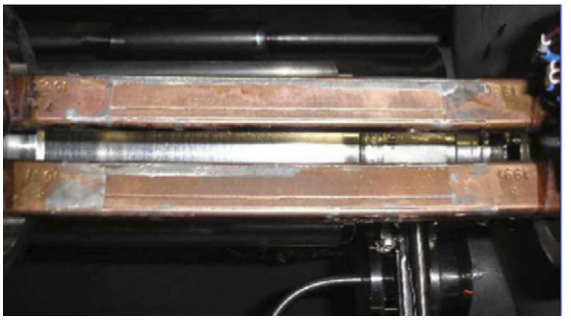

Fig. 20. Bus-bar as installed.

The decision was taken to operate for data taking at 3.5 TeV per beam until the end of 2011 and then in a shutdown in 2013 to repair and consolidate the splices [38] in such a way that they would be safe for maximum LHC energy and for all future upgrades of the machine.

6.2. Early operation

Following the repair and the hardware commissioning in 2009, there was a time slot of 26 days remaining before the end of the year. It was decided to use this time to operate with beam at a maximum dipole current of 2000 A which is equivalent to 1.18 TeV per beam. During this short test period, beams were injected in both rings, "stable beams" collisions (where the experimental detectors can be safely turned on) were performed at 450 GeV and beams were accelerated to 1.18 TeV per beam where a limited amount of physics data taking was performed.

First collisions

The day of the first collisions at 7 TeV center of mass energy was planned for March 30, 2010. The first two attempts at collisions resulted in beam losses for minor technical reasons. On the third attempt, the beams were successfully brought into collision [39]. The very first events with collisions at 7 TeV are shown for the four detectors in Fig. 21, and the first two physics runs at this energy are depicted in Fig. 22.

6.3. Progress in 2010

During 2010, operation was continuously divided between machine studies to increase the luminosity and physics data taking. The luminosity increase concentrated on increasing the current per bunch, the number of bunches and reducing the β^* in the collision points. The rate of progress was impressive, nevertheless before each step was taken to increase the intensity and hence the stored beam energy, all machine protection systems were validated up to the necessary level.

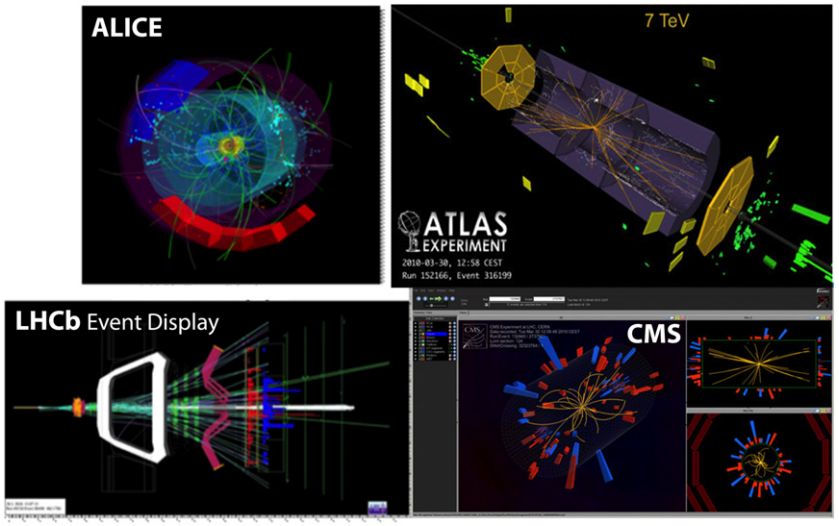

Fig. 21. Illustration of the first events recorded at 7 TeV CM energy in the four LHC detectors, as visible in the on-line event displays.

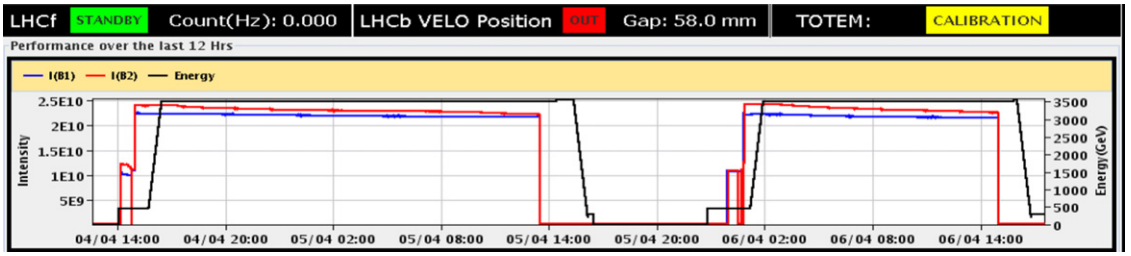

Fig. 22. First physics runs at 7 TeV CM (blue/red plot is intensity of: beam 1/2 respectively; black is the beam energy). (For interpretation of the references to colour in this figure legend, the reader is referred to the web version of this article.)

The LHC machine protection system [40] is probably one of the most intricate accelerator protection systems ever operated. It relies on very stringent control of the optics of the machine, both locally and globally. For all protection devices there are closed orbit constraints as well as β value constraints. Hence, any effects which are intensity dependent (e.g. closed orbit measurement, β^* measurement…) complicate the procedure for finalizing the protection. The collimation system [41] is part of the machine protection system and the collimators must intercept almost the totality of any beam losses if they are to protect the rest of the machine. The hierarchy of the collimation system (primary, secondary, and tertiary) must be respected. This implies a stringent control of the β functions and the closed orbits at the collimators and at all location with tight aperture margins, at all beam energies and throughout the "squeeze" of the low-β insertions [42] and the orbits are subjected to a feedback control with threshold limits. There is a watch-dog monitoring the orbit deviations at the locations of the collimators and if the limits are violated, the beam is dumped. A similar system is employed at the location of the beam dump extraction kicker. The tolerances set on the β "beating" (the relative deviation of the actual β's from their nominal values) is around 20% and Fig. 23 shows first measurements made at beam energies between 1.5 and 3.5 TeV [43]. In recent months (2011) the β "beating" has been corrected to below 10%, a factor of two better than the specifications.

In order to measure the cleaning efficiency of the collimation system, "loss maps" are made by provoking beam losses around the circumference. When the collimator jaws are well set up with the respect to the beam, and the hierarchy of losses is correct, the vast majority of all losses should be localized at the collimators in the warm cleaning insertions. Fig. 24 shows one of the early measurements where it can be seen that the ratio between the losses at the collimators and the worst cold location is about a factor of 10,000. It has been found that the optics and closed orbit remain within acceptable tolerances for periods of at least weeks without compromising the overall collimator hierarchy.

There are numerous examples of the high quality of the beam diagnostics systems and its implementation into the controls applications. Fig. 25 shows one such example. In order to measure the chromaticity during the energy ramp, the beam momentum is modulated by varying the RF frequency and the transverse tunes are measured by a phase lock loop [44,45].

Another early example is shown in Fig. 26, which shows the operation of orbit feedback during the energy ramp [46]. The maximum r.m.s. orbit change during the ramp is 0.08 mm compared to the design specifications of 0.5 mm r.m.s. and $\pm$4 mm peak orbit excursions.

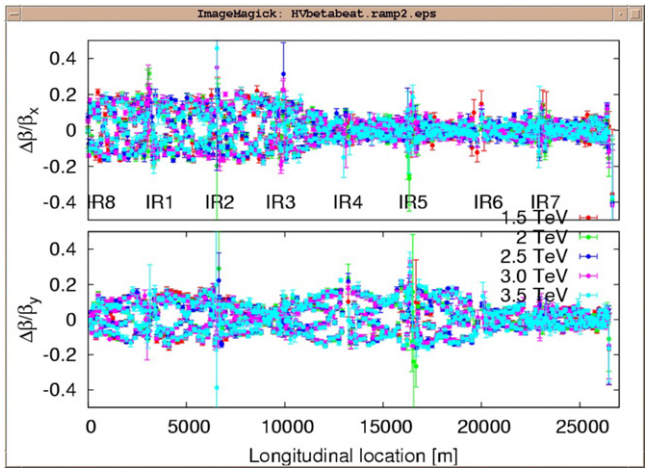

Fig. 23. Measurement of the β beating at different energies.

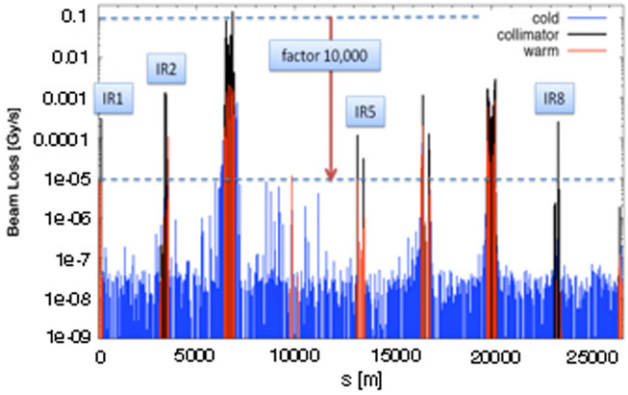

Fig. 24. Loss maps for collimation.

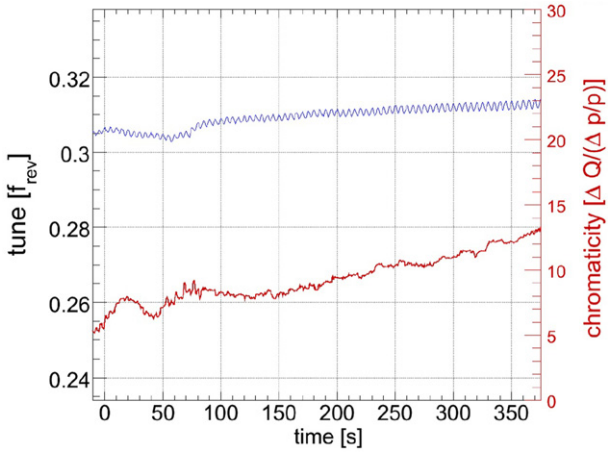

Fig. 25. Example of a vertical tune and chromaticity measurements during the energy ramp, (the upper blue plot shows the modulation of the tune and from the peak to peak of the modulation the chromaticity is calculated and shown in the lower red plot). (For interpretation of the references to colour in this figure legend, the reader is referred to the web version of this article.)

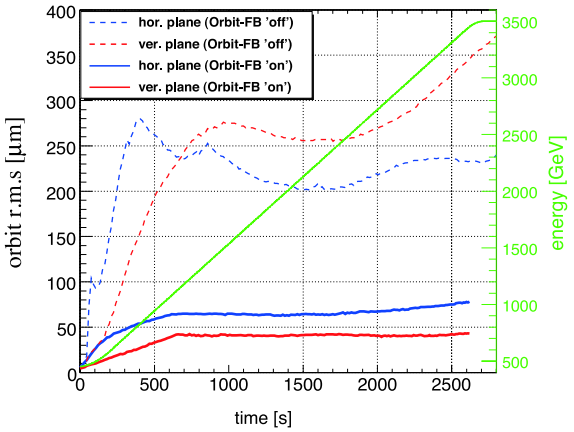

Fig. 26. Evolution of the measured r.m.s orbit deviation during the energy ramp with (solid) and without (dashed line) orbit feedback.

Table 4
Evolution of beam performance in 2010 (n_c is the number of bunches colliding). The main changes are highlighted with bold characters.

Event	E_b (TeV)	β^* (m)	n_b	$N_{1,2}$	E_{tot}(MJ)	n_c	L(cm^{-2}s^{-1})	Date
1	3.5	10	2	1×10^{10}	0.01	1	8.9×10^{26}	30/03/2010
2	3.5	10	2	$\mathbf{2 \times 10^{10}}$	0.02	1	3.6×10^{27}	02/03/2010
3	3.5	**2**	2	2×10^{10}	0.02	1	1.8×10^{28}	10/04/2010
4	3.5	2	**4**	2×10^{10}	0.05	2	3.6×10^{28}	19/04/2010
5	3.5	2	**6**	2×10^{10}	0.07	4	7.1×10^{28}	15/05/2010
6	3.5	2	**13**	2.6×10^{10}	0.19	8	2.4×10^{29}	22/05/2010
7	3.5	**3.5**	**3**	$\mathbf{1.1 \times 10^{11}}$	0.19	2	6.1×10^{29}	26/06/2010
8	3.5	3.5	**6**	1.0×10^{11}	0.34	4	1.0×10^{30}	02/07/2010
9	3.5	3.5	**8**	9.0×10^{10}	0.41	6	1.2×10^{30}	12/07/2010
10	3.5	3.5	**13**	9.0×10^{10}	0.66	8	1.6×10^{30}	15/07/2010
11	3.5	3.5	**25**	1.0×10^{11}	1.41	16	4.1×10^{30}	30/07/2010
12	3.5	3.5	**48**	1.0×10^{11}	2.71	36	9.1×10^{30}	14/08/2010

6.4. Operational performance in 2010

Protons 2010

As previously stated, LHC has been operating in shared mode between beam commissioning and physics data taking during 2010.

Table 4 shows the evolution of the beam performance from the first collisions in March until the middle of August (the first column give the machine status event number, and at each event there were several days of operation under these conditions). During the first period (events 1–6), the total number of bunches (column marked n_b) was increased from the initial value of 2–13 and the interaction region focusing parameter β^* was reduced to 2 m for most of the events. This progression in parameters produced an increase in the peak luminosity L of around a factor of 250 during this first data taking period.

For the second period (events 7–12), the number of protons per bunch in both beams $N_{1,2}$ was increased to near the design value of 1.15×10^{11}, the β^* was increased to 3.5 m to provide more margin in preparation of operation with crossing angle, and the number of bunches was progressively increased from 3 to 48. This progression resulted in peak luminosities reaching close to 10^{31} cm^{-2} s^{-1}. The total stored energy E_{tot} in each beam reached above 1 MJ (Megajoule) in event 11. From experience in previous accelerators it is known that this amount of stored energy is sufficient to puncture and melt fairly large sections of the vacuum chamber. Increase in the stored beam energy from this point onwards was only authorized after a rigorous protocol in the validation of the machine protection system.

In the third period of operation in 2010 "trains" of bunches from the injectors were used. This necessitated even more rigorous control and validation of the machine protection system for the injection of bunch trains. As can be seen in Table 5, the number of bunches per beam was increased from 56 to 368 from the end of September to the end of October, and the resulting peak luminosity reached 2×10^{32} cm^{-2} s^{-1}.

Fig. 27 shows the peak and integrated luminosity evolution during 2010 for proton operation. The initial goal of a peak luminosity of 10^{32} was exceeded by more than a factor of 2, and the integrated luminosity delivered to the experiments was 45 pb^{-1}. Following the series of fills with 368 bunches per beam, operation was switched to collisions of lead ions.

Table 5
Performance evolution with bunch trains.

n_b	$N_{1,2}$	E_{tot} (MJ)	n_c	L (cm^{-2} s^{-1})	Pile up	Date
56	1.10×10^{11}	3.5	47	2.0×10^{31}	1.91	30/03/2010
104	1.10×10^{11}	6.5	93	3.5×10^{31}	1.80	25/09/2010
152	1.10×10^{11}	9.4	140	5.0×10^{31}	1.76	29/09/2010
204	1.10×10^{11}	12.7	186	7.0×10^{31}	1.83	04/10/2010
248	1.10×10^{11}	15.4	233	1.03×10^{32}	2.22	14/10/2010
312	1.10×10^{11}	19.4	295	1.50×10^{32}	2.57	16/10/2010
368	1.15×10^{11}	23.9	348	2.05×10^{32}	2.97	25/10/2010

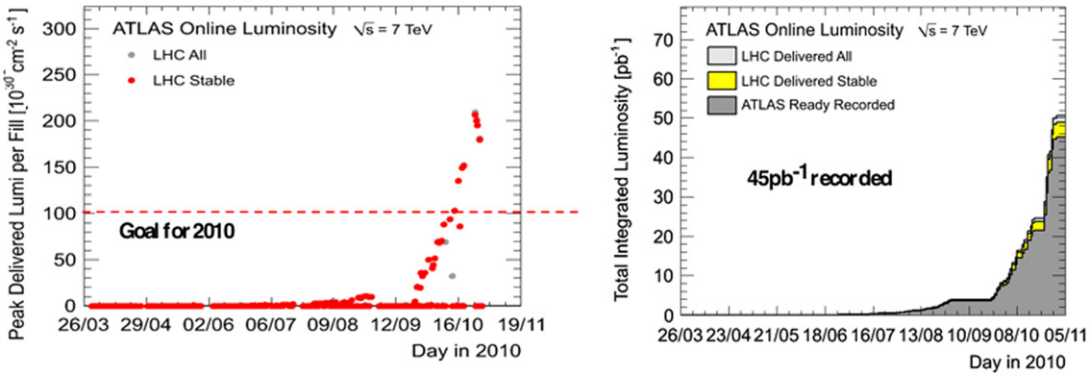

Fig. 27. Peak and integrated luminosity during 2010.

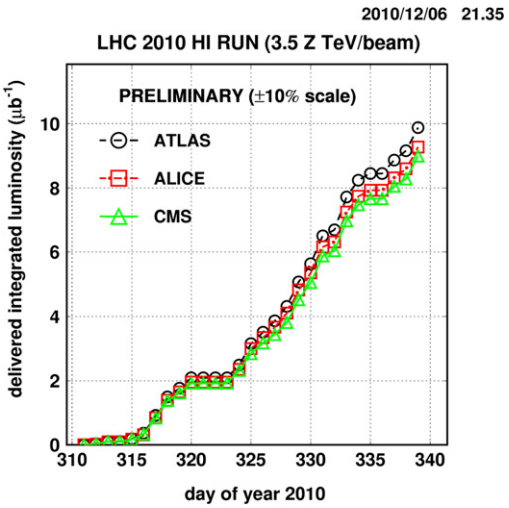

Fig. 28. Integrated luminosity for the lead ion operation during 2010.

Lead ions in 2010

The change-over from protons to lead ions went extremely efficient, taking only 4 days to produce colliding lead ions. Operation of the LHC with lead ions was performed for about 4 weeks and produced luminosities well above expectations. The integrated luminosities are shown as a function of date in Fig. 28.

6.5. Proton operation in 2011

Contrary to the mode of operation in 2010, the strategy for operation in 2011 was to separate operations for physics data taking from the machine studies. The goal set for 2011 was to produce an integrated luminosity of at least 1 fb^{-1}; more than 20 times that achieved in 2010. Towards the end of 2010 while injecting a couple of hundred bunches per beam, clear signs of beam and vacuum instabilities appeared which are produced by the electron cloud effect. This effect had been predicted for the LHC and the mitigation foreseen was to perform "beam cleaning" or "scrubbing" [47] Beam cleaning requires large numbers of high intensity bunches circulating for extended periods so as to generate an electron cloud build-up but still

Table 6
Evolution of peak performance in 2011.

Fill number	Date	Bunch spacing	Number of bunches	Peak luminosity (10^{33} cm^{-2} s^{-1})	Total number of protons per beam (10^{14})
1635	18 March 2011	75	32	0.03	0.04
1637	19 March 2011	75	64	0.06	0.07
1644	22 March 2011	75	136	0.17	0.16
1645	22 March 20l1	75	200	0.25	0.24
1712	15 April 2011	50	228	0.24	0.29
1716	16 April 2011	50	336	0.35	0.42
1739	26 April 2011	50	480	0.51	0.58
1749	30 April 2011	50	624	0.72	0.76
1755	02 May2011	50	768	0.83	0.93
1809	27 May2011	50	912	1.10	1.15
1815	29 May2011	50	1092	1.27	1.33
1901	27 June 2011	50	1236	1.25	1.64
2032	18 August 2011	50	1380	2.40	1.68

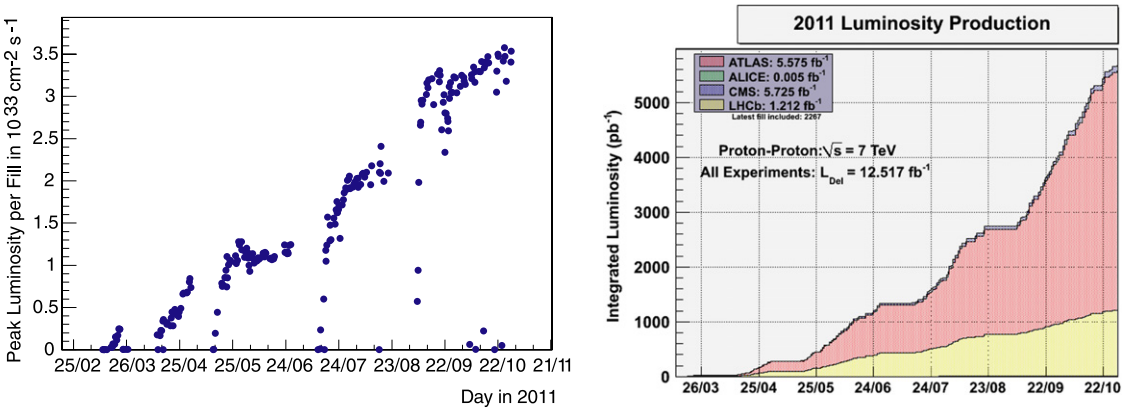

Fig. 29. Peak and Integrated luminosity during 2011.

allow stable beam operation below the heat load threshold for the cryogenic system. The resulting surface treatment by the electron bombardment eventually reduces the secondary electron yield of the vacuum tube thereby allowing increasingly higher intensities of circulating protons.

The global strategy for operation in 2011 was firstly to re-establish the good performance of 2010 with up to several hundred bunches, followed by beam cleaning and then to increase the number of bunches towards 900 (maximum achievable with a bunch spacing of 75 ns). The beam cleaning was done with bunch spacings of 50 ns in order to increase the effectiveness of the cleaning. Following the successful beam cleaning runs with 50 ns spacing it was decided that physics operation could continue with 50 ns bunch spacing thereby increasing the potential maximum number of bunches to close to 1400. In order to allow the accumulation of such large numbers of bunches, the number of bunches in the bunch trains coming from the injectors had to be increased. In the first half of the year the trains of bunches were increased progressively from 12 to 144, each step carefully validated by a machine protection panel.

Table 6 shows the evolution of the number of bunches per beam in the LHC during the period from mid-March until mid-August. For physics data taking, the maximum number of bunches reached to this date is 1380 (this is the maximum achievable with a bunch spacing of 50 ns) with a total number of protons reaching 1.68×10^{14} and a peak luminosity of 2.4×10^{33} cm^{-2} s^{-1}. The energy stored in this high intensity beam is more than 100 MJ.

Fig. 29 shows the evolution of the integrated (right) and peak luminosity during 2011. It can be seen that the 2011 goal of 1 fb^{-1} was achieved very early in the year and exceeded by more than a factor of 5 towards the end of the 2011 run. Fig. 30 shows details of the most productive fill to date with an integrated luminosity of 122 pb^{-1} in 15 h. This greatly exceeded the totality of the production of 45 pb^{-1} in 2010.

The record performances up to mid-October 2011 are detailed in Table 7. It should be noted that the peak luminosity at 7 TeV center of mass is significantly in excess of the design luminosity at this energy.

The beam conditions for the experiments in the LHC are generally very good. Luminosity and background signals from the experiments are available online in the LHC control room. Machine induced background levels rarely exceed 1% of the signal from proton–proton collisions for the high luminosity experiments (ATLAS and CMS) [48].

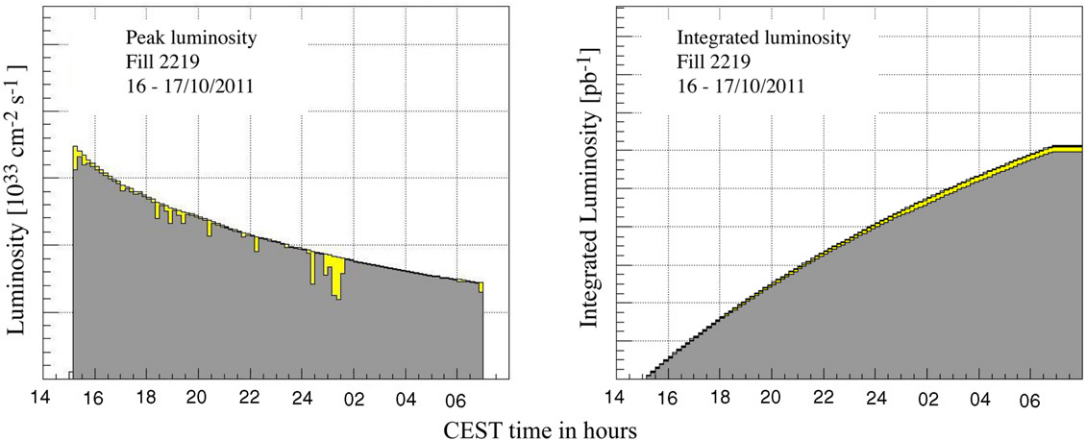

Fig. 30. Peak, integrated luminosity during the best fill to date.

Table 7
Records as of October 14, 2011.

Peak stable luminosity delivered	3.5×10^{34} cm^{-2} s^{-1}	Fill 2219, 16/10/2011, 06:14
Maximum luminosity delivered in one fill	122.44 pb^{-1}	Fill 2219, 16/10/2011
Maximum luminosity delivered in one day	135.45 pb^{-1}	13/10/2011
Maximum luminosity delivered in 7 days	546.25 pb^{-1}	10–16/10/2011
Maximum number of colliding bunches	1331	Fill 1956, 18/07/2011
Maximum number events per bunch crossing	29.83	Fill 2201, 10/10/2011, 07:59
Longest time in stable beams for on fill	26 h	Fill 2206, 05/08/2011
Longest time in stable beams for one day	21.9 h (91.2%)	03/08/2011
Longest time in stable beams for 7 days	107.1 h (63.7%)	03–09/08/2011
Fastest turnaround to stable beams	2.11 h	Fill 2032, 17/08/2011

6.6. Plans for the end of 2011 and 2012

Towards the end of 2011, operation is reverted to colliding lead ions, again for about one month. In 2012 LHC will continue operation at or slightly above 3.5 TeV per beam with the goal of maximizing the integrated luminosity before the machine shuts down for a long period in 2013–2014. During this long shut-down the inter-magnet connectors will be repaired and upgraded by an improved design. Several other consolidation programs are foreseen during this shutdown both for the LHC and the injectors. Following this shutdown the goal is to operate close to 7 TeV per beam with high intensity beams.

7. Upgrade considerations

7.1. Upgrade motivation and planned stages

The startup of the LHC advanced at an impressive pace in 2010 and 2011 and came within a factor three of its nominal target performance at reduced beam energies (3.5 TeV instead of the nominal 7 TeV beam energies).

This high initial performance level is to a large extend based on the better then expected performance of some key LHC systems: beam instrumentation, controls, magnet model and the collimation system to just to name a few.

The luminosity was increased by operating with smaller than nominal transverse beam emittances ($\epsilon_n = 2.5\ \mu$m compared to the nominal design value of $\epsilon_n = 3.75\ \mu$m) and higher than nominal bunch intensities (1.4×10^{11} particles per bunch compared to the nominal value of 1.15×10^{11}). This increased the strength of the head-on beam–beam interaction beyond nominal, but did not cause any problems in beam lifetime or emittance growth.

Mechanical imperfections and tolerances in the triplet magnets were found to be lower than anticipated during the LHC design phase, resulting in an increased aperture allowing for reduced β^* values [49].

However, in spite of this initial success, the machine development must stay focused on planning for an even further performance increase over the coming decades. The goal for the LHC performance evolution is to keep the halving time for the statistical error of the physics data within a reasonable time interval (of the order of 10 years). Halving the statistical error implies a four fold increase in the total number of recorded events in the detectors, implying an increase of the machine performance by a factor 2–4 every 5–10 years.

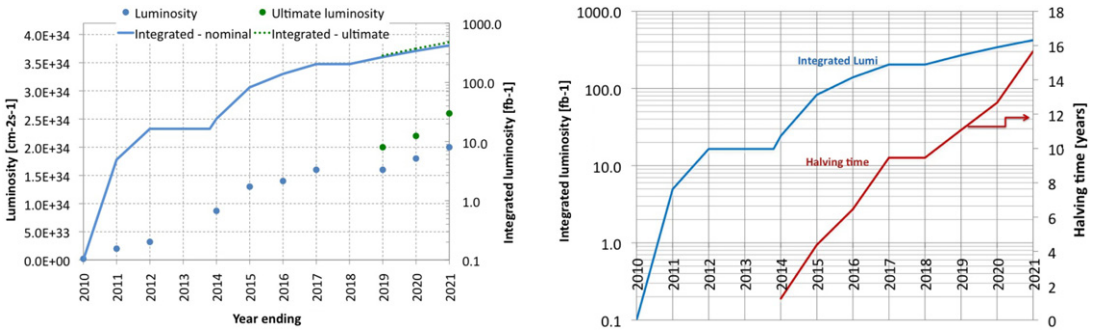

Fig. 31. Left: Projected evolution of the LHC luminosity over the coming decade. Right: The resulting evolution of the integrated luminosity for the LHC experiments and the corresponding halving time for the statistical error of the LHC physics data.

Two long shutdowns are planned for increasing the LHC performance beyond its nominal design goal of a peak luminosity of $L = 10^{34}$ cm^{-2} s^{-1} before 2020:

- Long Shutdown 1 (LS1) in 2013 for consolidating the LHC inter-magnet splice connections and allowing operation of the LHC at nominal beam energies of 7 TeV. The energy increase is expected to provide an approximately four fold increase of the peak luminosity (factor 2 from the increased energy and a factor 2 from the smaller β^* values that are accessible at 7 TeV), resulting in a peak luminosity above the design value of $L = 10^{34}$ cm^{-2} s^{-1} at otherwise identical beam parameters from the 2011 operation.
- Long Shutdown 2 (LS2) in 2018 for connecting the new LINAC4 accelerator to the CERN PSB and for consolidating the LHC and its injector chain for operation above nominal beam brightness (bunch intensity divided by transverse beam emittance) with 25 ns bunch spacing and upgrading the LHC experiments for being able to digest the resulting higher event rates. This should allow either ultimate bunch intensities at nominal beam emittances or the 2011 bunch parameters for 25 ns bunch spacing. This second upgrade stage should therefore provide approximately another factor two increase of the peak luminosity with respect to the operation after LS1 to $L \approx 2.5 \times 10^{34}$ cm^{-2} s^{-1}.

Fig. 31 shows the evolution of the peak and integrated luminosity per experiment over time assuming the LHC performance exceeds already the nominal performance after LS1 thanks to the ability of operating the LHC with smaller than nominal beam emittances but remains around $L = 2.5 \times 10^{34}$ cm^{-2} s^{-1} after LS2 [50]. The right-hand side of Fig. 31 shows in addition to the integrated luminosity also the evolution of the halving time of the statistical error. Without an additional performance increase of the LHC beyond LS2, the halving time for the statistical error of the experiments exceeds a reasonable length of ∼10 years by 2019. CERN has therefore launched two upgrade projects for pushing the performance of the LHC even further, aiming at a further two to three fold increase in the yearly integrated luminosity:

- The LHC Injector Upgrade Project LIU. The goal is to surpass current limitations of the existing LHC injector complex, to be able to deliver the high brightness beams required for the HL-LHC.
- The High Luminosity upgrade project HL-LHC. The goal is to allow for a luminosity production of 200–300 fb^{-1} per year.

The LIU and HL-LHC upgrade modifications are planned to be implemented during a third long shutdown LS3 in 2022.

In addition to the above medium term projects, CERN has engaged in superconducting magnet R&D efforts aiming at a further increase of the beam energies (doubling of the nominal LHC beam energies) by using higher field magnets in the existing LHC tunnel [51].

7.2. The HL-LHC upgrade goals

Peak instantaneous luminosity and luminosity leveling

Operation with nominal LHC performance of $L = 10^{34}$ cm^{-2} s^{-1} and 25 ns bunch spacing implies for the main experiments a mean pileup of approximately 20 events per bunch crossing. It is assumed that the detectors could digest an event pileup of ∼100 events per bunch crossing with a significant detector upgrade. Higher pileup rates are considered as too challenging and the HL-LHC upgrade project therefore aims at a peak luminosity of $L = 5 \times 10^{34}$ cm^{-2} s^{-1} during operation. In order to meet the HL-LHC goal of an integrated luminosity of 200–300 fb^{-1} per year, the HL-LHC upgrade relies on luminosity leveling which is a technique to intentionally reduce the instantaneous luminosity as a function of the beam intensity which finally gives a constant luminosity level during a run. The machine parameters for the HL-LHC are further tailored for a peak luminosity well above $L = 5 \times 10^{34}$ cm^{-2} s^{-1}, but where the actual luminosity during the collider operation is kept constant at $L = 5 \times 10^{34}$ cm^{-2} s^{-1} by a continuous adjustment of the operational parameters. This procedure avoids too high event pileup rates in the experiments while maximizing the integrated luminosity over a fill. The following procedures and tools are considered for the luminosity leveling [52]:

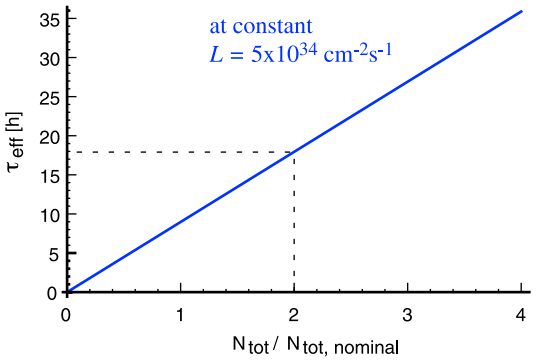

Fig. 32. The variation of the beam lifetime in a high luminosity collider as a function of the beam current for total hadronic cross section of $\sigma_{\text{tot}} = 100$ mb for collisions in 2 IPs.

- Transverse offsets of the beams at the IP.
- The use of Crab cavities for manipulating the beam overlap of the two beams in the luminous region.
- Manipulation of the external crossing angle of the two beams (e.g. with the help of partial compensation of the long-range beam–beam interactions in the common vacuum system with the help of wires).
- A dynamic change of the β-functions at the IPs.
- Bunch length variation

The operation with luminosity leveling can be maintained as long as the beam currents in the machine are compatible with luminosity values higher than the target leveled luminosity L_{Lev}.

Assuming that the beam burn off due to the particle collisions is the dominant loss mechanism for the beams during the HL-LHC operation, the beam lifetime can be written as:

$$\frac{dN(t)}{dt} = -n_{\text{IP}}\,\sigma_{\text{tot}}\,L_{\text{Lev}} = -\frac{N_{\text{ini}}}{\tau_{\text{eff}}}, \tag{11}$$

where n_{IP} is the number of high luminosity IPs in the machine, σ_{tot} the total hadronic cross section for collisions at the IPs and where we have introduced τ_{eff} as the effective beam lifetime. The time dependence of the beam current is then given by:

$$N(t) = (1 - t/\tau_{\text{eff}})\ N_{\text{ini}}. \tag{12}$$

Fig. 32 shows the resulting beam lifetime for a total hadronic cross section of $\sigma_{\text{tot}} = 100$ mb and a leveled luminosity of $L_{\text{Lev}} = 5 \times 10^{34}\ \text{cm}^{-2}\ \text{s}^{-1}$ as a function of the beam current. Assuming that the LHC can be operated with beam currents twice as large as those for the nominal design parameters (doubling the bunch intensity to 2.3×10^{11} particles per bunch) [53] the upper limit for the effective beam lifetime would be 18 h.

For a given beam-overlap size, the luminosity depends quadratically on the beam current and the luminosity leveling can be sustained for a time

$$T_{\text{leveling}} = \left(1 - 1/\sqrt{k}\right)\ \tau_{\text{eff}}, \tag{13}$$

where τ_{eff} is the effective beam lifetime for the leveled luminosity and k specifies the virtual luminosity reach of the collider

$$L_{\text{virtual}} = k\,L_{\text{Lev}}. \tag{14}$$

Assuming a maximum beam intensity of 5×10^{14} protons per beam ($\sim$1 A beam current), one obtains a beam lifetime of $\tau_{\text{eff}} = 13.9$ hours. Assuming further a virtual luminosity reach in the HL-LHC that is a factor 4 higher than the target leveled luminosity ($k = 4$ and $L_{\text{virtual}} = 20 \times 10^{34}\ \text{cm}^{-2}\ \text{s}^{-1}$) one obtains a maximum leveling time of 7 h. The above discussion underlines that the HL-LHC project aims at the highest possible beam currents and the maximum possible virtual peak luminosity. In the following we assume a maximum total beam intensity of 5×10^{14} protons per beam ($\sim$1 A beam current) and a virtual luminosity reach in the HL-LHC that is a factor 4 higher than the target leveled luminosity ($k = 4$). The integrated luminosity with leveling is simply given by the product of the leveled luminosity and the leveling time:

$$L_{\text{int}} = L_{\text{Lev}}\ \left(1 - \sqrt{L_{\text{Lev}}/L_{\text{virtual}}}\right). \tag{15}$$

For a virtual luminosity of $L_{\text{virtual}} = 20 \times 10^{34}\ \text{cm}^{-2}\ \text{s}^{-1}$ ($k = 4$) and a maximum beam intensity of 5×10^{14} protons per beam ($\tau_{\text{eff}} = 13.9$ h), one obtains a leveling time of 7 h and an integrated luminosity of $L_{\text{int}} > 1.25\ \text{fb}^{-1}$ per fill. Extending the run at the end of the leveling until the luminosity has dropped to half the leveled luminosity value, generates an additional $0.4\ \text{fb}^{-1}$ over 3 h. The total run length is then given by the leveling time plus 3 h (which is 10 h for 5×10^{14} protons per beam and $k = 4$) and the total integrated luminosity per fill reaches approximately $1.65\ \text{fb}^{-1}$.

Table 8 lists the attainable integrated luminosity values for different virtual peak luminosity values.

Table 8
Integrated luminosity values per fill for a leveled luminosity of $L_{\text{level}} = 5 \times 10^{34}\ \text{cm}^{-2}\ \text{s}^{-1}$, a total beam current of 5×10^{14} protons per beam and different virtual to peak luminosity ratios $k = L_{\text{virtual}}/L_{\text{Lev}}$.

$k = L_{\text{virtual}}/L_{\text{level}}$	Run length, (h)	L_{int}/fill, (fb^{-1})
1	3	0.4
2	7.1	1.13
4	10	1.65

Limits for β^* values

The smallest attainable β^* values are limited by the available triplet aperture and by chromatic aberration arising from the corresponding large β-function values in the triplet magnets left and right from the IP.

Assuming an operation with crossing angle (and a beam separation of $10\,\sigma$) the triplet aperture must provide space for approximately 30 beam sigma. Adding additional margins for β-beat and dispersion offsets, the aperture requirement can be approximated by

$$A \geq 35\,\sigma + \delta_{\text{mech}}, \tag{16}$$

where δ_{mech} specifies additional aperture margins for mechanical tolerances which are independent from the beam size in the triplet magnets. As illustrated in Section 5, the beam size in the triplet magnets increases inversely proportional to the beam divergence at the IP:

$$\sigma_{\text{trip}} \propto \frac{1}{\sqrt{\beta^*}}. \tag{17}$$

The nominal LHC triplet configuration is compatible with an operation with $\beta^* = 0.5$ m featuring gradients of 200 T/m and magnet apertures of 60 mm diameter. The nominal LHC triplet configuration corresponds to peak magnetic fields of more than 6 T at the magnet coils which is at the limit of the NbTi technology. Reducing the β-function at the IP to below $\beta^* = 0.5$ m either implies the use of magnet technologies that are compatible with higher peak magnetic fields at the coils (e.g. Nb_3Sn magnet technology) or the use of triplet magnets with lower gradients. The use of lower triplet gradients implies in turn even larger peak β-functions inside the triplet magnets for a given β^* value. Both options are being considered for the HL-LHC upgrade plans with the goal of operating the HL-LHC with $\beta^* \leq 0.25$ m.

Scaling the peak β-functions inside the triplet magnets for the nominal LHC configuration with $\beta^* = 0.5$ m to $\beta^* = 0.25$ m implies peak beta function values of more than 9 km. Considering furthermore triplet gradients of less than 200 T/m for the upgrade triplet configuration, the peak β-functions can easily exceed values of 13 km.

The chromatic aberrations of a quadrupole magnet are directly proportional to the peak β-function inside the magnet. For the nominal LHC configuration, the chromatic correction systems are compatible for operation with $\beta^* \geq 0.3$ m. Smaller β^* values require special optics configurations that partially compensates the chromatic aberrations from different IPs and enhances the corrector strength in the arcs by increasing the β-functions [54]. One such configuration, the "Achromatic Telescopic Squeezing" scheme, has already been successfully demonstrated in special LHC machine studies and has been adopted as the baseline solution for the HL-LHC operation with $\beta^* \leq 0.3$ m. For the HL-LHC baseline configuration we assume $\beta^* = 0.2$ m.

Geometric reduction factor for an operation with crossing angle

The two counter-rotating beams collide in the LHC with a crossing angle in order to avoid unwanted head-on collisions in the common vacuum beam pipe away from the actual Interaction Point (IP). Instead of colliding head-on at these unwanted collision points, the bunches of the two counter-rotating beams pass each other with a transverse offset. The nominal LHC features approximately 30 of these long range beam–beam encounters per Interaction Region (IR) for operation with 25 ns bunch spacing. The tune spread due to the long-range beam–beam interactions depends on the crossing angle amplitude and the resulting beam separation at the parasitic beam encounters in the IRs. The nominal crossing angle configuration in the LHC aims at a minimum beam separation of $10\,\sigma$ at these long range collision points.

The required full crossing angle between the two beams inside the common beam pipe near the IP can be written as:

$$\tan\phi \approx 10\sqrt{\frac{\epsilon_n}{\beta^*\gamma}}. \tag{18}$$

The crossing angle results in a reduction of the luminosity via an effective increase of the cross section at which the two beams intersect with each other and a reduction of the luminous region. This geometric luminosity reduction is schematically illustrated in Fig. 33.

The geometric luminosity reduction factor can be written for round beams as [2]

$$F = \sqrt{\frac{1}{1+\Theta^2}}, \tag{19}$$

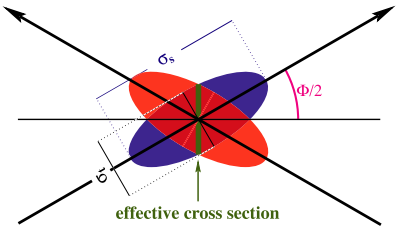

Fig. 33. Two beams crossing at the angle Φ. The effective beam overlap cross-section is increased compared to the transverse beam size σ_t.

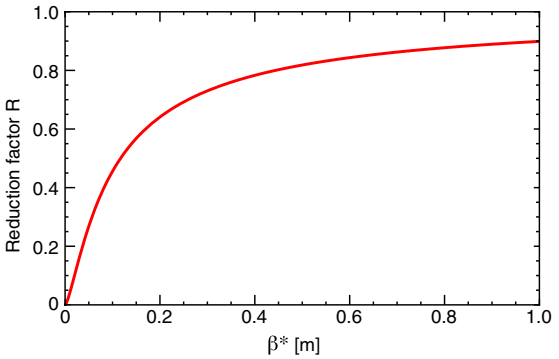

Fig. 34. The geometric luminosity reduction factor as a function of β^* for a crossing angle corresponding to a beam separation of $10\,\sigma$, for the nominal bunch length of 7.55 cm and $\epsilon_n = 3.75$ μm.

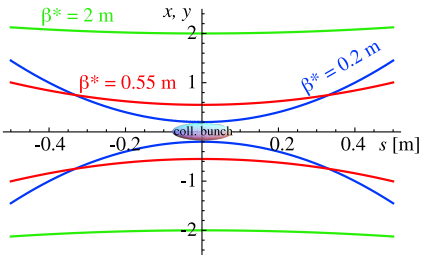

Fig. 35. Illustration of the hour-glass effect for a β^* of 2 m, the nominal 0.55 and 0.2 m as considered for the LHC upgrade. For small β^*, the variation of the β-function over the bunch length of the colliding bunches becomes non-negligible.

where we have introduced the Piwinski parameter

$$\Theta = \frac{\phi\sigma_s}{2\sigma_t}, \tag{20}$$

where σ_s is the r.m.s. bunch length and σ_t the transverse r.m.s. bunch size in the plane of the crossing angle. Fig. 34 shows the resulting geometric luminosity reduction factor as a function of β^*. The reduction of 15% at $\beta^* = 0.5$ m can still be considered as moderate. The reduction of 50% for $\beta^* \leq 0.2$ m would be significant and motivates studies for compensation using Crab cavities.

A further reduction in luminosity comes from the hour-glass effect, which is illustrated in Fig. 35. The luminosity gets reduced by the factor $H(r)$,

$$H(r) = \frac{1}{\sqrt{\pi}} \int_{-\infty}^{\infty} \frac{e^{-s^2}}{1 + s^2/r^2}\, ds, \tag{21}$$

where $r = \beta^*/\sigma_s$. The effect was negligible for the LHC commissioning with $\beta^* \geq 1$ m. At the nominal LHC parameters, it results in a reduction of the luminosity by 1% ($\beta^* = 0.55$ m, $\sigma_s = 7.55$ cm, $H = 0.99$). At $\beta^* = 0.2$ m, we have $H = 0.94$, i.e. a luminosity reduction by 6% from the hour-glass effect.

Maximizing the single bunch intensity and the beam–beam limit

The single bunch limitation for the Transverse Mode Coupling Instability (TMCI) is estimated to be of the order of 3.5×10^{11} particles per bunch [19] and can be considered as an upper limit for the accessible bunch intensities for the LHC.

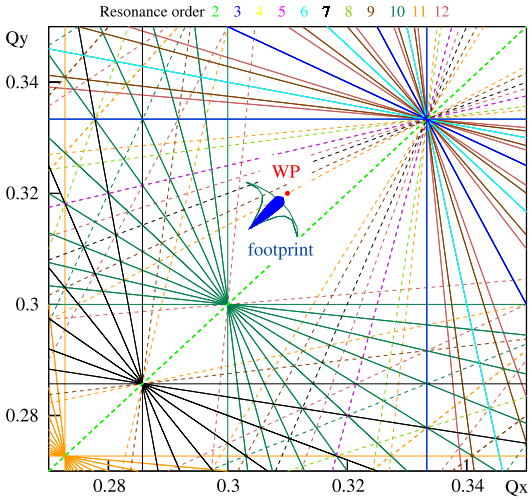

Fig. 36. The LHC working point "WP" and beam–beam tune spread "footprint" of the LHC in the tune diagram. Resonances up to 12th order are shown. Sum resonances are shown with solid lines and difference resonances as dashed lines.

Another limitation for the beam intensity arises from the beam–beam interaction. The strength of the beam–beam interaction can be characterized by the linear head-on beam–beam parameter which specifies the maximum tune shift due to the beam–beam interaction per IP that a particle at the center of a bunch experiences when the two bunches collide without a crossing angle and transverse offset. The particle tune is defined as the number of oscillations a particle performs on average over one revolution in the storage ring. The beam–beam parameter is given by

$$\xi_{x,y} = \frac{N_b\, r_p\, \beta^*_{x,y}}{2\pi\, \gamma\, \sigma_{x,y}\, (\sigma_x + \sigma_y)}, \tag{22}$$

where γ is the relativistic gamma factor and r_p the classical proton radius $r_p = e^2/(4\pi\epsilon_0 mc^2)$.

For round beams with equal beam emittances in both planes, the beam–beam force is independent of the transverse β-functions at the IP and depends only on the normalized beam emittance. For round beams the beam–beam parameter can be written as:

$$\xi = \frac{N_b\, r_p}{4\pi\, \epsilon_n} \tag{23}$$

where ϵ_n is the normalized emittance.

While the beam–beam force in the LHC acts like a linear defocusing element (quadrupole), the force becomes strongly non-linear for particle amplitudes around $1.5\,\sigma$ of the beam size and changes it's slope for large amplitude particles (long range beam–beam encounters) where the beam–beam force corresponds to the force generated by a charged wire.

The beam–beam limit in hadron colliders without strong synchrotron radiation damping is loosely referred to as the maximum acceptable total tune spread that can still be accommodated in the tune diagram without exposing particles of the beam to too strong resonances. Experience of previous colliders has shown that resonances of order 12 or lower are detrimental to the beam distribution, where a resonance is defined as

$$m\, Q_x + n\, Q_y = p \tag{24}$$

with m, n, p being integers. The order of the resonance is defined as the sum of the absolute values of the integers m and n. The beam–beam limit can therefore be estimated as the maximum tune spread that can be accommodated in the tune diagram without exposing particles within the beam to resonances of order 12 or lower. Fig. 37 shows the nominal tune spread in the LHC due to beam–beam interactions in the transverse tune diagram together with resonance lines of up to 12th order.

The LHC working point is placed between the 1/3rd and 3/10th resonance and particles can experience the 4/13th and 5/16th or higher order resonances. Fig. 36 shows schematically the LHC working point and beam–beam tune spread of the LHC in the tune diagram. Depending on the required distance to the coupling and sextupole (1/3rd tune) resonance, the overall required resonance-free space in the tune space (depends on whether 10th order resonances need to be avoided or can be tolerated for some particle amplitudes) varies between 0.01 and 0.03. The nominal LHC parameters feature a maximum total beam–beam tune spread of $\Delta Q = 0.01$ (for bunches colliding in three experiments and with three head-on collisions) and are compatible with the requirements of avoiding 10th order resonances, conservative margins for the coupling strength and allowing for additional sources for tune spread in the LHC. The observed beam–beam limit in the *Sp$\bar{p}$S* collider was approximately $\Delta Q = 0.018$ and the beam–beam limit in the Tevatron collider is approximately $\Delta Q = 0.02$ for the anti-proton beam.

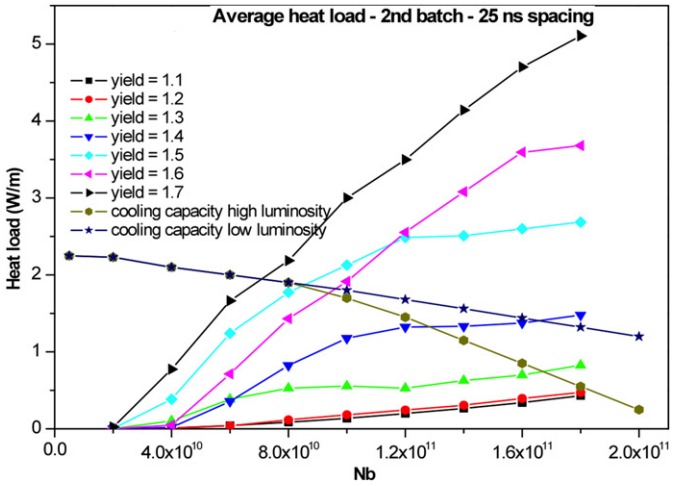

Fig. 37. The expected heat load in the cold section of the LHC from simulations for 25 ns bunch spacing as a function of the bunch intensity and for different values of the secondary emission yield.

Higher values have been achieved in the Tevatron (values of $\Delta Q = 0.03$ have been reached) but the experimental conditions and beam performance degraded quickly in the Tevatron for beam–beam tune shifts larger than $\Delta Q = 0.02$ [55]. The LHC operation experience in 2010 has shown that a total maximum beam–beam tune shift of up to $\Delta Q = 0.025$ (three collisions per bunch) can be achieved in routine luminosity runs with a bunch spacing of 50 ns instead of the nominal 25 ns bunch spacing (half the number of long range beam–beam encounters) [21]. Even higher beam–beam tune shifts of up to $\Delta Q = 0.03$ have been obtained during special machine studies.

Assuming in the following a beam–beam limit of $\Delta Q = 0.025$, one can use Eq. (23) to estimate the maximum acceptable beam brightness in the LHC from the beam–beam point of view. For three head on collisions (in ATLAS, CMS and LHCb) and nominal beam emittance, the resulting maximum acceptable bunch intensity corresponds approximately to the TMCI limit from single bunch collective effects. Assuming smaller than nominal beam emittances (e.g. $\epsilon_n = 2.5\ \mu$m instead of the nominal $\epsilon_n = 3.75\ \mu$m) the maximum acceptable bunch intensities might be smaller.

These estimates do not yet include the effect of the geometric reduction factor which reduces not only the luminosity but also the beam–beam tune shift. With alternating crossing angles, the geometric reduction factor reduces the luminosity and the beam–beam tune-shift by approximately the same factors and the limits for the bunch intensity from the beam–beam point of view will remain above those from the TMCI collective effects even for smaller than nominal beam emittances. In the following we can therefore assume that the TMCI collective effect imposes the most stringent limits on the single bunch intensities.

Maximizing the number of bunches

The number of bunches in the LHC can be limited by the electron-cloud effect [23]. Electrons in the beam vacuum chamber (either originating from electron desorption via synchrotron radiation or electrons coming from residual gas ionization processes) are accelerated by the positively charged proton beams and release secondary electrons after impact on the vacuum chamber walls. These secondary electrons are then accelerated by the following bunches and the resulting electron cloud can drive beam instabilities, heat the beam screen in the cryogenic sections and deteriorate the vacuum in the warm sections of the LHC. The LHC operation with more than 300 bunches showed in 2010 clear signs for the onset of electron cloud activity and the operation with more than 300 bunches required dedicated conditioning of the vacuum surfaces in the LHC. The electron bombardment of the beam pipe surfaces results in a reduction of the secondary electron yield. The vacuum surfaces can therefore be conditioned by so called "beam scrubbing" runs as long as the electron cloud density is compatible with a safe beam operation in the LHC. Fig. 37 shows the expected heat load in the cold section of the LHC from simulations for 25 ns bunch spacing as a function of the bunch intensity and for different values of the secondary emission yield [56].

Even for a very efficient "beam scrubbing" and low secondary emission yields of $\delta_{SY} = 1.1$, the heat load from the electron cloud effect comes close to the limit of the cryogenic cooling capacity in the LHC arcs (indicated by the line "cooling capacity low luminosity") for bunch intensities reaching $N_b \approx 2 \times 10^{11}$ protons. The limits coming from the cryogenic cooling capacity of the triplet magnets are indicated by the curve labeled "cooling capacity high luminosity". These limits will be addressed by a dedicated upgrade of the cryogenic systems for the triplet magnets within the HL-LHC upgrade project. The limits in the arc are given by the maximum He flow rates within the cooling capillaries of the beam screen and are directly given by the diameter of the cooling capillaries. For the HL-LHC beam parameters, we assume an optimistic "beam scrubbing" scenario, in which the secondary emission yield of the LHC vacuum system can be lowered to $\delta_{SY} = 1.1$ by the time of the HL-LHC operation and assume for the HL-LHC beam parameters for operation with 25 ns bunch spacing maximum bunch intensities of $N_b = 2 \times 10^{11}$ protons.

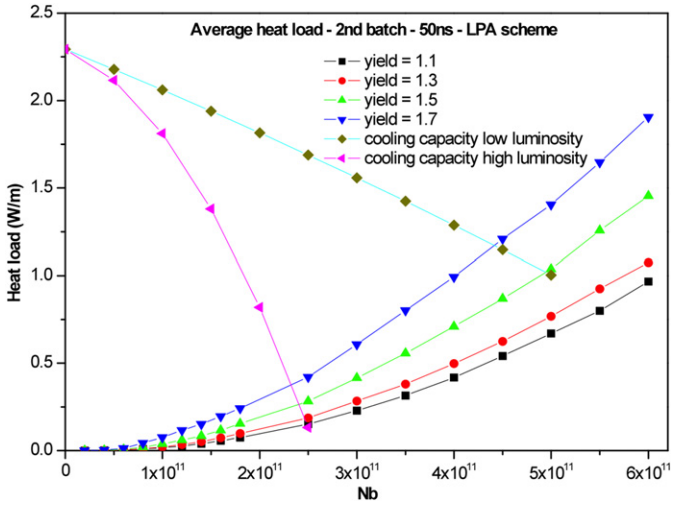

Fig. 38. The expected heat load in the cold section of the LHC from simulations for 50 ns bunch spacing as a function of the bunch intensity and for different values of the secondary emission yield.

Fig. 38 shows the expected heat load in the cold section of the LHC from simulations for 50 ns bunch spacing as a function of the bunch intensity and for different values of the secondary emission yield [56]. For 50ns bunch spacing, the maximum heat load stays within the capacities of the arc cryogenic cooling system even for rather inefficient "beam scrubbing" scenarios and secondary emission yields of $\delta_{SY} \leq 1.7$. The maximum acceptable bunch intensities are in this case larger than the limits imposed by collective effects ($N_b = 3 \times 10^{11}$ protons per bunch (ppb) from the Transverse Mode Coupling Instability). Until it has been demonstrated that secondary emission yields of $\delta_{SY} \leq 1.1$ are attainable with "beam scrubbing" in the LHC, we keep the 50 ns bunch spacing operation mode as a backup option for the HL-LHC beam configurations.

7.3. Summary of the HL-LHC performance reach

Table 9 summarizes the maximum performance reach for the LHC machine when considering the increased beam brightness from a complete injector complex upgrade and operation with small β^* values [54]. The table shows the nominal design parameters together with two sets of HL-LHC parameters: one for operation with 25 ns and one for operation with 50 ns. The 50 ns option produces a pileup of over 200 events per crossing, which would be very difficult for the experiments.

Both HL-LHC upgrade parameter sets given in Table 9 clearly exceed the design goal for the peak luminosity of the HL-LHC project ($L = 5 \times 10^{34}$ cm^{-2} s^{-1}) (by ∼15%–20% without additional compensation of the geometric reduction factor) and a factor two margin with leveling (geometric reduction factor $R < 0.5$) if one considers leveling options via Crab cavities and beam–beam long-range wire compensators that allow operation with smaller crossing angles.

It is interesting to note, that for both options with larger than nominal bunch intensities, the total beam–beam tune shift remains well below $\Delta Q = 0.02$ if one assumes three IPs and assumes that the tune shift arising from the long-range beam–beam interactions is much smaller than the tune shift coming from the head-on collisions. The total beam current for the operation with 50 ns bunch spacing remains below the "ultimate" beam current of 0.85 A. The beam current for the 25 ns option exceeds this assumed maximum value by approximately 20%.

7.4. Summary

The above performance evaluations show that the design goal of the HL-LHC project can only be achieved with a full upgrade of the injector complex and the operation with β^* values below 0.25 m. Significant margins for leveling can only be achieved for β^* values close to 0.2 m. However, these margins can only be harvested during the HL-LHC operation if the required leveling techniques have been demonstrated to be operational. Options for leveling include:

- The use of Crab cavities (not yet demonstrated for operation of hadron storage rings).
- The use of wire compensators for compensating the long-range beam–beam interaction. While it has been experimentally demonstrated that wires have a measurable effect on the stability of halo particles it has not yet been demonstrated that wires can compensate beam–beam induced long-range collisions in operation. It is therefore desirable to install long range beam–beam wire compensators during the first long shutdown of the LHC (currently scheduled for 2013–2014) so that their applicability can be experimentally investigated in the LHC before the implementation of the HL-LHC upgrade (currently planned at the earliest for 2020).

Table 9
LHC performance reach at 7 TeV with HL-LHC and a full injector complex upgrade compared to the nominal parameters.

Parameter	Nominal	25 ns	50 ns
N_b (10^{11})	1.15	2.0	3.3
n_b	2808	2808	1404
I (A)	0.58	1.01	0.83
β^* (m)	0.55	0.2	0.2
ϵ_n (μm)	3.75	2.5	3.75
ϵ_s (eV s)	2.5	2.5	2.5
E spread	1.13×10^{-4}	1.13×10^{-4}	1.13×10^{-4}
σ_s (cm)	7.55	7.55	7.55
IBS h (htbp)	106	25	37
IBS l (htbp)	60	21	21
b–b sep. (σ)	10	10	10
Φ (μrad)	300	420	520
Piwinski Θ	0.647	1.17	1.96
Geom. Reduct. R	0.840	0.459	0.455
Hour-glass H	0.99	0.94	0.94
b-b ξ (10^{-3})	3.1	4.2	4.6
Event pileup, $\sigma = 60$ mb	19	123	221
L (cm^{-2} s^{-1})	1×10^{34}	6.5×10^{34}	5.8×10^{34}

- Dynamic squeeze of the optic functions at the IP during luminosity operation. Feasibility of such a procedure has never been demonstrated during operation of an existing machine, not to mention for a machine like the LHC with unprecedented stored beam energies and small margins for losses during operation. An experimental validation of this option would be very interesting for the planning of the HL-LHC upgrade.
- Luminosity leveling via transverse offsets of the beams at the IPs. While first operation experience in the LHC has shown that the operation with beam offsets at the IP is in principle possible, the feasibility of such a procedure has never been demonstrated during operation with many long range beam–beam interactions. An experimental evaluation of this option would be very interesting for the planning of the HL-LHC upgrade.

Assuming a maximum limit for the total beam current in the LHC, the performance can clearly be maximized by putting the beam current in the smallest number of bunches. This gives a preference for operation with 50 ns bunch spacing. However, the operation with 50 ns bunch spacing also implies larger bunch luminosities and therefore a larger event pileup per interaction. While the event pileup is approximately 100 for the operation scenarios with 25 ns bunch spacing (approximately a factor fife larger than the nominal pileup), the maximum event pileup varies between 150 and 240 events per bunch crossing for the operation scenarios with 50 ns bunch spacing corresponding approximately to a tenfold increase with respect to the nominal LHC configuration. It still remains to be demonstrated that such high pileup rates are acceptable for the experiments.

Acknowledgments

This paper summarizes the work carried out by hundreds if not thousands of scientists, engineers and technicians both employed by CERN and very importantly by the many institutes that collaborate with CERN. It is a great personal pleasure to acknowledge the incredible contributions and dedication of such a wonderful team.

References

[1] O. Brüning, et al. (Ed.), LHC design Report. Vol. 1–3. CERN-2004-003-V-1–3. http://ab-div.web.cern.ch/ab-div/Publications/LHC-DesignReport.html.
[2] W. Herr, B. Muratori, Concept of luminosity, in: Proc. CAS2003, CERN-2006-002 p. 361. http://doc.cern.ch/yellowrep/2006/2006-002/p361.pdf.
[3] D. Brandt, H. Burkhardt, M. Lamont, S. Myers, J. Wenninger, Rep. Progr. Phys. 63 (2000) 939. http://iopscience.iop.org/0034-4885/63/6/203/pdf/r006r3.pdf.
[4] V. Shiltsev, Achievements and lessons from tevatron, in: Proc. IPAC 2011. http://accelconf.web.cern.ch/AccelConf/IPAC2011/papers/tuya01.pdf.
[5] S. Myers, W. Schnell, Preliminary performance estimates for a LEP proton collider; LEP Note 440; April 1983. http://cdsweb.cern.ch/record/443058.
[6] Recommendation by the High Energy Physics Advisory Panel (HEPAP) in 1983 for "immediate initiation of a multi-TeV high-luminosity proton–proton collider project with the goal of physics experiments at this facility at the earliest possible date.", SSC history. http://www.hep.net/ssc/new/history/appendixa.html.
[7] A. Asner, et al., DIR-TECH/84-01 & ECFA 84/85, CERN 84-10. http://cdsweb.cern.ch/record/152775.
[8] V. Shiltsev, Modern Phys. Lett. A 25 (2010) 567–577. 1003.3051. http://xxx.lanl.gov/abs/1003.3051.
[9] G. Brianti, Experience with the CERN p anti-p complex, in: Proc. PAC, 1983. http://accelconf.web.cern.ch/AccelConf/p83/PDF/PAC1983_1950.PDF.
[10] K. Johnsen, The ISR and accelerator physics, CERN-84-13, 1984. http://cdsweb.cern.ch/record/156665.
[11] G.A. Voss, B.H. Wiik, Annu. Rev. Nucl. Part. Sci. 44 (1994) 413–452. http://nucl.AnnualReviews.org/cgi/content/abstract/44/1/413.
[12] M. Harrison, T. Ludlam, S. Ozaki, Nucl. Instrum. Meth. A 499 (2003) 235–244.
[13] ATLAS Collaboration, G. Aad, et al., J. Instrum 3 (2008) S08003.
[14] CMS Collaboration, R. Adolphi, et al., J. Instrum 3 (2008) S08004.
[15] LHCb Collaboration, J. Alves, A. Augusto, et al., J. Instrum 3 (2008) S08005.
[16] ALICE Collaboration, K. Aamodt, et al., J. Instrum 3 (2008) S08002.

[17] L. Rossi, Experience with LHC magnets from prototyping to large-scale industrial production and integration, in: Proc. EPAC 2004. http://accelconf.web.cern.ch/AccelConf/e04/PAPERS/WEXCH01.PDF.
[18] P. Schmüser, Prog. Part. Nucl. Phys. 49 (2002) 155–244.
[19] E. Metral, Pushing the limits-beam, in: Proc. Chamonix Workshop, 2011. http://cdsweb.cern.ch/record/1353867.
[20] W. Herr, D. Kaltchev, Results of dynamic aperture studies for increased beta* with beam–beam interactions, LHC-Project-Note-416. http://cdsweb.cern.ch/record/1114615.
[21] W. Herr, et al., Observations of beam–beam effects at high intensities in the LHC, in: Proc. IPAC 2011. http://accelconf.web.cern.ch/AccelConf/IPAC2011/papers/weoda01.pdf.
[22] O. Gröbner, CERN-ISR-VA-77-38, CERN June 1977. http://cdsweb.cern.ch/record/314892.
[23] F. Zimmermann, A simulation study of electron-cloud instability and beam-induced multipacting in the LHC, CERN-LHC-Project-Report-95. http://cdsweb.cern.ch/record/323928.
[24] H. Burkhardt, R. Schmidt, Intensity and luminosity after beam scraping, CERN-AB-2004-032. http://doc.cern.ch/archive/electronic/cern/preprints/ab/ab-2004-032.pdf.
[25] G. Papotti, A beam quality monitor for LHC beams in the SPS, in: Proc. EPAC 2008, THPC144. http://accelconf.web.cern.ch/AccelConf/e08/papers/thpc144.pdf.
[26] P. Letnes, et al., Beam scraping to detect and remove halo in LHC injection, in: Proc. EPAC 2008, THPC149. http://accelconf.web.cern.ch/AccelConf/e08/papers/thpc149.pdf.
[27] H. Burkhardt, et al., Collimation in the transfer lines to the LHC, in: Proc. PAC 2005, TPAP009. http://cern.ch/AccelConf/p05/PAPERS/TPAP009.PDF.
[28] V. Kain, et al., Protection level during extraction, transfer and injection into the LHC, in: Proc. PAC 2005, RPPE016. http://cern.ch/AccelConf/p05/PAPERS/RPPE016.PDF.
[29] B. Goddard, Expected beam delivery precision of the injected LHC beam, LHC Project Note 337, CERN February 2004. http://cdsweb.cern.ch/record/719045.
[30] B. Goddard, M. Barnes, et al., Emittance growth at LHC injection from SPS and LHC kicker ripple, in: Proc. EPAC 2008, THPP113. http://accelconf.web.cern.ch/AccelConf/e08/papers/thpp113.pdf.
[31] R. Assmann, Collimation for the LHC high intensity beams, in: Proc. of HB2010, MOIB03. http://hb2010.web.psi.ch/proceedings/papers/moib03.pdf.
[32] S. Van der Meer, Calibration of the effective beam height in the ISR, CERN-ISR-PO-68-31, CERN 1986.
[33] S. White, H. Burkhardt, Luminosity Calibration at the CERN Large Hadron Collider using the Van der Meer method, PRSTAB (2012) (submitted for publication).
[34] M. Bajko, et al., Report of the task force on the incident of 19 September 2008 at the LHC, LHC Project Report 1168, CERN March 2009. http://cdsweb.cern.ch/record/1168025.
[35] V. Baglin, et al., Recovering about 5 km of LHC beam vacuum system after sector 3–4 incident, in: Proc IPAC 2010, THPEA086. http://accelconf.web.cern.ch/AccelConf/IPAC10/papers/thpea086.pdf.
[36] F. Formenti, et al., Upgrade of the quench protection systems for the superconducting circuits of the LHC machine at CERN: from concept and design to the first operational experience, in: Proc IPAC 2010, MOPD013. http://accelconf.web.cern.ch/AccelConf/IPAC10/papers/mopd013.pdf.
[37] M. Koratzinos, et al., High-current bus splice resistances and implications for the operating energy of the LHC, in: Proc IPAC 2010, MOPEB044. http://accelconf.web.cern.ch/AccelConf/IPAC10/papers/mopeb044.pdf.
[38] F. Bertinelli, et al., Towards a consolidation of LHC superconducting splices for 7 TeV operation, in: Proc IPAC 2010, MOPEB042. http://accelconf.web.cern.ch/AccelConf/IPAC10/papers/mopeb042.pdf.
[39] K. Fuchsberger, et al., Operational experience during initial beam commissioning of the LHC, in: Proc IPAC 2010, MOPEC007. http://accelconf.web.cern.ch/AccelConf/IPAC10/papers/mopec007.pdf.
[40] R. Schmidt, J. Wenninger, Initial experience with the machine protection system for the LHC, in: Proc IPAC 2010, TUOCMH03. http://accelconf.web.cern.ch/AccelConf/IPAC10/papers/tuocmh03.pdf.
[41] D. Wollmann, et al., First cleaning with LHC collimators, in: Proc IPAC 2010, TUOAMH01. http://accelconf.web.cern.ch/AccelConf/IPAC10/papers/tuoamh01.pdf.
[42] R. Steinhagen, et al., Continuous measurement and control of beta-beating in the LHC, in: Proc IPAC 2010, MOPE062. http://accelconf.web.cern.ch/AccelConf/IPAC10/papers/mope062.pdf.
[43] R. Tomas, et al., LHC optics model measurements and corrections, in: Proc IPAC 2010, TUXMH02. http://accelconf.web.cern.ch/AccelConf/IPAC10/papers/tuxmh02.pdf.
[44] R. Steinhagen, et al., Influence of varying tune width on the robustness of the LHC tune PLL and its application for continuous chromaticity measurement, in: Proc PAC 2007, MOPAN074. http://accelconf.web.cern.ch/AccelConf/p07/PAPERS/MOPAN074.PDF.
[45] L. Arnaudon, et al., Operation experience with the LHC RF system, in: Proc IPAC 2010, TUPEB056. http://accelconf.web.cern.ch/AccelConf/IPAC10/papers/tupeb056.pdf.
[46] R. Steinhagen, et al., Commissioning and initial performance of the LHC beam-based feedback systems, in: Proc IPAC 2010, WEPEB041. http://accelconf.web.cern.ch/AccelConf/IPAC10/papers/wepeb041.pdf.
[47] V. Baglin, et al., Observations of electron cloud effects with the LHC vacuum system, in: Proc IPAC 2011, TUPS018. http://accelconf.web.cern.ch/AccelConf/IPAC2011/papers/tups018.pdf.
[48] Y. Levinsen, et al., Fill analysis and experimental background observations in the LHC, in: Proc IPAC 2011, TUPZ020. http://accelconf.web.cern.ch/AccelConf/IPAC2011/papers/tupz020.pdf.
[49] R. Assmann, et al., Aperture determination in the LHC based on an emittance blowup technique with collimator position scan, in: Proc. IPAC 2011, TUPZ006. http://accelconf.web.cern.ch/AccelConf/IPAC2011/papers/tupz006.pdf.
[50] HL-LHC: high luminosity large hadron collider. http://hilumilhc.web.cern.ch/HiLumiLHC/.
[51] Proc. HE-LHC10 Workshop, CERN-2011-003, Malta, 2010. http://cdsweb.cern.ch/record/1344820.
[52] F. Zimmermann, HL–LHC: parameter space, constraints & possible options, in: Chamonix 2011 Proc., p. 295. http://cdsweb.cern.ch/record/1341525.
[53] R. Assmann, Implications of higher intensities in the LHC, in: Proc. Chamonix 2010. https://espace.cern.ch/acc-tec-sector/Chamonix/Chamx2010/papers/RA_9_02.pdf.
[54] S. Fartoukh, Breaching the phase *I* optics limitations for the HL–LHC, in: sLHC Project Report 0053, CERN January 2011. http://cdsweb.cern.ch/record/1364853.
[55] V. Shiltsev, et al., Beam-beam effects in the Tevatron. PhysRevSTAB.8.101001.
[56] H.M. Cuna, et al., Simulations of electron-cloud heat load for the cold arcs of the LHC and its high-luminosity upgrade scenarios, PRST-AB (2012) (submitted for publication).